Sinonasal Cavities

9

Prashant Raghavan, Mark J. Jameson, Max Wintermark, and Sugoto Mukherjee

9.1 Anatomy and Physiology

9.1.1 Nose and Nasal Cavity

The bony skeleton of the nose is formed by the nasal bones and the nasal processes of the maxillae. The nasal septum is comprised of the septal cartilage anteriorly, the vomer posteroinferiorly and the perpendicular plate of the ethmoid bone superiorly. The Kiesselbach's/Little's area is located in the anterior/inferior septum, and this is where branches of the sphenopalatine, greater palatine, and facial arteries anastomose; it is the most common site of epistaxis.

The piriform aperture is the anterior bony opening of the nasal cavity. The posterior choana is the posterior opening, divided in the midline by the vomer.

The roof of the nasal cavity is formed by the cribriform plate of the ethmoid bone. The floor is formed anteriorly by the palatine processes of the maxilla and posteriorly by the horizontal processes of the palatine bones.

Three meati (spaces) are present along the lateral wall of the nasal cavity lateral to the superior, middle, and inferior turbinates. They contain the sites of drainage of the paranasal sinuses.

9.1.2 Paranasal Sinuses

There are three or four turbinates, designated as supreme (variable), superior, middle, and inferior. The inferior turbinate is a separate bone, while the other three are parts of the ethmoid bone. The middle turbinate is attached to the lateral nasal wall by the basal lamella, which separates the anterior and posterior ethmoid air cells. The space between the basal lamella and the ethmoid bulla is the sinus lateralis or suprabullar recess (Fig. 9.1).

The lateral nasal wall is comprised of two ostiomeatal units. The anterior ostiomeatal unit consists of the frontal sinus ostium, frontal recess, maxillary sinus

P. Raghavan et al., *Manual of Head and Neck Imaging*,
DOI 10.1007/978-3-642-40377-4_9, © Springer-Verlag Berlin Heidelberg 2014

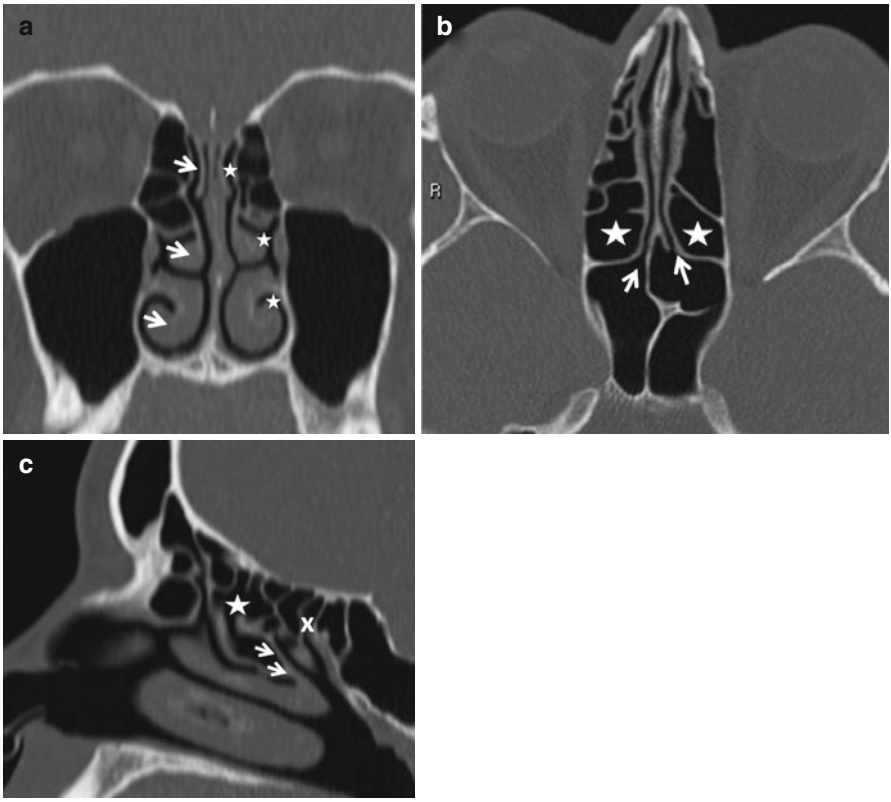

Fig. 9.1 (**a**) The 3 *arrows* point to the superior, middle, and inferior turbinates. The 3 *asterisks* indicate the corresponding meati. (**b**) The *arrows* point to the ostia of the sphenoid sinus, which open into the sphenoethmoidal recesses. The *asterisks* indicate the posterior ethmoid air cells. (**c**) The *arrows* indicate the basal or ground lamella of the middle turbinate, which separates the anterior (*asterisk*) from the posterior ethmoid air cells (*x*)

ostium, infundibulum, and middle meatus. The posterior ostiomeatal unit is comprised of the sphenoid sinus ostium, sphenoethmoidal recess, and the superior meatus (Fig. 9.1).

The uncinate process is a sickle-shaped sheet of bone arising from the lateral nasal wall and directed superiorly. Lateral to the superior free edge is the infundibulum. The ethmoid bulla is the largest anterior ethmoid air cell. Its medial wall forms the lateral wall of the infundibulum. The infundibulum is the air passage bounded medially by the uncinate process and laterally by the ethmoid bulla; it connects the maxillary sinus ostium to the middle meatus. The hiatus semilunaris is the crescentic gap between the free edge of the uncinate process and the ethmoid bulla (Fig. 9.2).

The frontal recess is the funnel-like drainage pathway of the frontal sinus. The term "frontonasal duct" is now avoided as no discrete ductal structure exists. The frontal recess drains into the anterior part of the middle meatus and may be divided into a superior compartment that lies below the frontal sinus ostium in the floor of

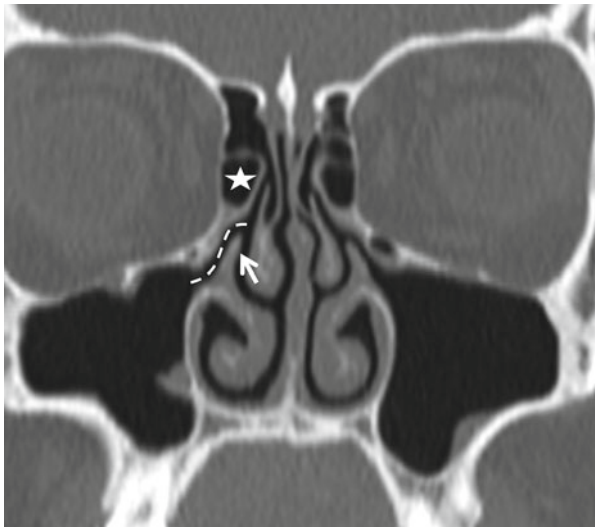

Fig. 9.2 The *curved dashed arrow* represents the infundibulum. Its medial opening is the hiatus semilunaris. It is bounded by the uncinate process (*arrow*) medially and the bulla ethmoidalis (*asterisk*) laterally

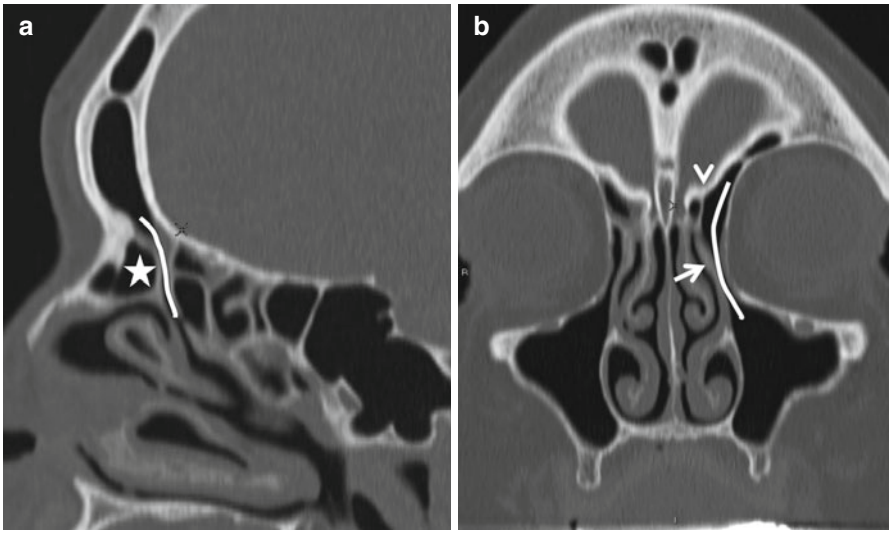

Fig. 9.3 The frontal sinus drainage pathway. The *curved lines* represent the frontal recess. An agger nasi (*asterisk*) cell is seen anterior to the frontal recess in (**a**). In (**b**), note that the uncinate process (*arrow*) is attached superiorly to the fovea ethmoidalis (*arrowhead*). This results in the frontal recess opening into the infundibulum

the sinus and an inferior compartment which either opens into the infundibulum (if the uncinate process is directed towards the skull base) or continues into the middle meatus (if the uncinate process is attached to the lamina papyracea) (Fig. 9.3).

The fovea ethmoidalis is the roof of the ethmoid cavity. The cribriform plates are the portion of the ethmoid bone that forms the roof of the nasal cavity medial to the

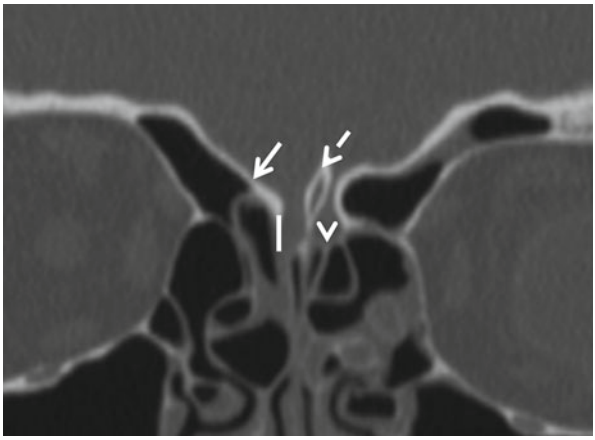

Fig. 9.4 Roof of the nasal cavity. The *arrow* points to the fovea ethmoidalis and the *arrowhead* to the cribriform plate. The *vertical line* represents the depth of the floor of the anterior fossa. The Keros system classifies this as type 1 where the depth is 1–3 mm, type 2 where the depth is 4–7 mm, and type 3 where the depth is between 8 and 11 mm. The greater the depth, the greater the potential for injury during endoscopic surgery. The cribriform plates may be dehiscent, as is the case on the right. The *dashed arrow* indicates the crista galli, to which the falx cerebri is attached. Occasionally the crista may be pneumatized and rarely contain a mucocele

Box 9.1. Paranasal Sinus Drainage

Frontal sinus	Through frontal recess into middle meatus
Anterior ethmoid cells	Middle meatus, mainly into infundibulum
Posterior ethmoid cells	Sphenoethmoidal recess (superior meatus)
Maxillary sinus	Through infundibulum into middle meatus
Sphenoid sinus	Sphenoethmoidal recess (superior meatus)

fovea ethmoidalis. They are perforated by the foramina of the olfactory nerves. The crista galli is a vertically oriented midline ridge of bone arising from the cribriform plates and attaching to the falx cerebri (Fig. 9.4). The anterior and posterior ethmoid air cells are separated by the basal lamella of the middle turbinate. The lamina papyracea is the gracile medial wall of the orbit. The agger nasi designates the most anterior ethmoid cells that form due to pneumatization into the lacrimal bone and the frontal process of the maxillae. They may be anterior, inferior, or posterolateral to the frontal recess and may encroach upon it (Fig. 9.3).

The sphenoethmoidal recess is the site of drainage of the sphenoid and posterior ethmoid air cells (Fig. 9.1).

A summary of sinus drainage is provided in Box 9.1.

Box 9.2. Anatomic Variations

- Nasal septal deviation
- Middle turbinate
  - Paradoxical curvature
  - Concha bullosa
- Uncinate process
  - Pneumatization (uncinate bulla)
  - Variable attachment of free edge to lamina papyracea (atelectatic)/fovea ethmoidalis
- Giant ethmoid bulla
- Lamina papyracea dehiscence
- Variations in ethmoid pneumatization
  - Haller cells
  - Onodi cells
  - Supraorbital cells
  - Frontal cells
  - Agger nasi cells
- Accessory maxillary sinus ostia
- Cribriform plates
  - Variability in depth
  - Dehiscence
- Sphenoid sinus
  - Attachment of septum to lateral wall adjacent to the ICA
  - Lateral wall dehiscence
  - Anterior clinoid process pneumatization

9.1.3 Anatomic Variations of Clinical Importance

The commoner anatomic variations are listed in Box 9.2.

The *nasal septum* is deviated in 25–30 % of the population. Marked deviation, especially with an osteocartilaginous spur, may compromise the middle meatus and predispose to recurrent sinonasal inflammation/infection (Fig. 9.5).

The *middle turbinate* may be completely pneumatized (concha bullosa) or pneumatized only within its vertical portion (lamellar concha or intralamellar air cell). Concha bullosae may become inflamed and rarely transform into a mucocele. In addition to conchae, paradoxically curved middle turbinates may also crowd the middle meatus leading to maxillary sinus obstruction (Fig. 9.6).

The free edge of the *uncinate process* may attach to the lamina papyracea (atelectatic uncinate) resulting in a chronically obstructed maxillary sinus ostium and hypoplasia of the maxillary sinus with associated descent of the orbital floor (silent sinus syndrome) (Fig. 9.7). If not recognized preoperatively, the plunging roof of the maxillary sinus may be inadvertently breached by the surgeon. The uncinate process may attach superiorly to the fovea ethmoidalis, in which case excessive traction during surgery may result in violation of the anterior cranial fossa and a CSF leak. The uncinate

Fig. 9.5 Nasal septal deviation. Septal deviation may predispose one to recurrent sinus inflammatory disease. The sharp leftward deviation in this case has resulted in hypoplasia of the middle turbinate and uncinate process and consequently a narrow infundibulum

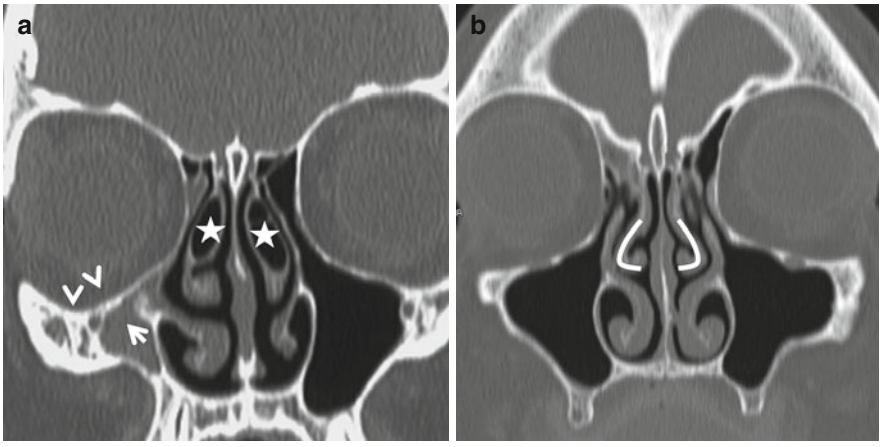

Fig. 9.6 (**a**) Concha bullosa. Pneumatization of the middle turbinates (concha bullosa, *asterisks*) is a fairly common anatomic variation and when substantial, can narrow the middle meatus. In (**a**), note that the right uncinate process (*arrow*) is deviated laterally (atelectatic) closing off the infundibulum, resulting in an obstructed, hypoplastic maxillary antrum. The right orbital floor has descended (*arrowheads*) and is at risk for injury during surgery. When accompanied by enophthalmos, this entity is referred to as the silent sinus syndrome. In (**b**), note that the convexity of the middle turbinates is directed laterally (*curved lines*) rather than towards the midline (paradoxical curvature). This can theoretically compromise the middle meatus

process may also be pneumatized (uncinate bulla), which encroaches upon the infundibulum and impedes frontal and anterior ethmoid sinus drainage (Fig. 9.7).

A *giant ethmoid bulla* is an unusually large ethmoidal bulla that compromises the infundibulum (Fig. 9.7).

Haller cells are infraorbital ethmoidal air cells. They may narrow the infundibulum and predispose patients to recurrent maxillary sinusitis (Fig. 9.8).

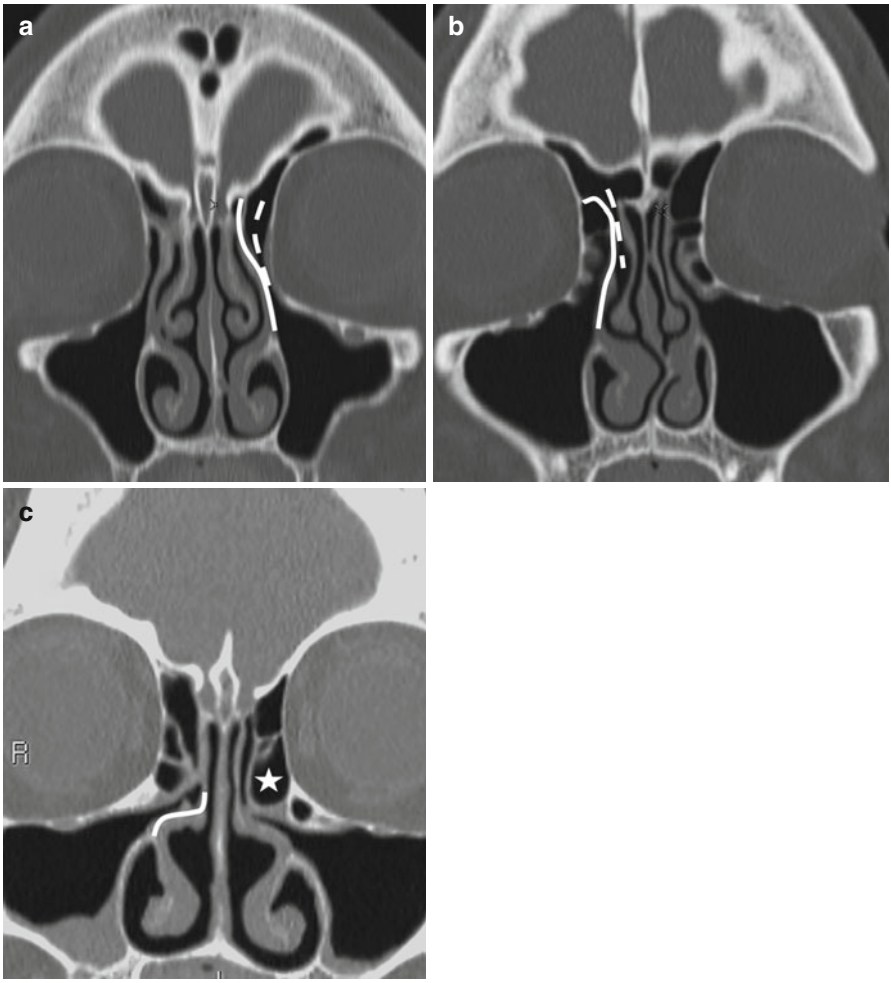

Fig. 9.7 Variations in uncinate process (UP) attachment. In (**a**), the uncinate process is attached superiorly to the fovea ethmoidalis (*continuous line*), resulting in the frontal recess opening into the infundibulum (*dashed line*). This configuration means that infundibular obstruction can result in simultaneous disease in the frontal, maxillary, and anterior ethmoid air cells. In (**b**), the UP is attached to the lamina papyracea (*continuous line*), resulting in the frontal recess (*dashed line*) draining into the middle meatus. This implies that the frontal and anterior ethmoid sinus drainage pathways are separated. Also, traction upon the UP during surgery may result in injury to the delicate lamina. In (**c**), the *continuous line* indicates attachment of the UP to the middle turbinate. The *asterisk* indicates a large ethmoid bulla, likely the cause of the UP being rotated medially

Onodi cells are the most posterior ethmoid air cells and are intimately related to the optic canal; they can completely surround the optic nerve, increasing the risk of optic nerve injury at surgery. Onodi cell mucoceles may compress the optic nerve (Fig. 9.8).

The *sphenoid sinus* is usually divided by a single sagittal septum, but multiple septa may be present. Sphenoid septa that insert laterally adjacent to the cavernous internal carotid artery may be associated with arterial injury at surgery. Pneumatization of the

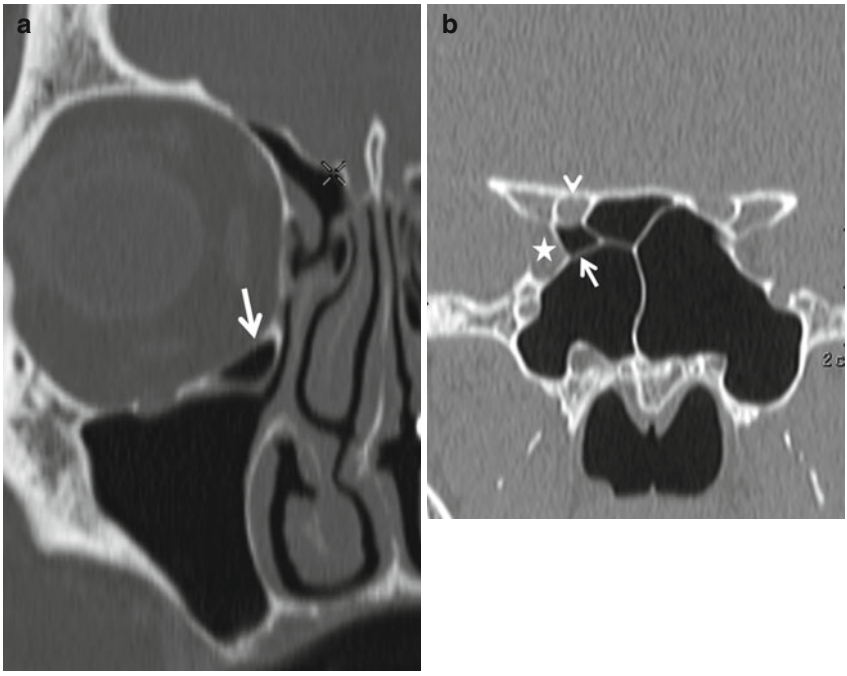

Fig. 9.8 (**a**) A Haller cell (*arrow*) represents an infraorbital ethmoid air cell and can compromise the infundibulum. (**b**) Onodi cells (*arrow*) result from posterior ethmoid pneumatization extending superior and lateral to the sphenoid sinus. These cells lie in close proximity to the optic nerves and occasionally, the internal carotid arteries, structures that may be injured if these cells are violated. Infection in an Onodi cell may also spread to the orbital apex rapidly. The *arrowhead* points to the optic canal and the *asterisk* indicated the superior orbital fissure

sphenoid sinus may extend into the anterior clinoid process and the horizontal carotid canals conferring increased risk of surgical injury to the optic nerves and internal carotid arteries, respectively. The lateral sphenoid sinus walls are occasionally dehiscent allowing the optic nerves and internal carotid arteries to pass through the sinus (Fig. 9.9).

9.1.4 Physiology

The nasal cycle is a normal, cyclical side-to-side alteration in nasal airway resistance. It can be associated with mucosal hypertrophy, which is detectable on CT and MR imaging, especially around the inferior turbinate; this must not be mistaken for pathology (Fig. 9.10).

9.2 Imaging Evaluation

Inflammatory sinonasal disease is evaluated most effectively by CT. Contrast is not usually required, except when spread of infection or inflammation beyond the sinonasal cavities into the orbits or adjacent soft tissues is suspected.

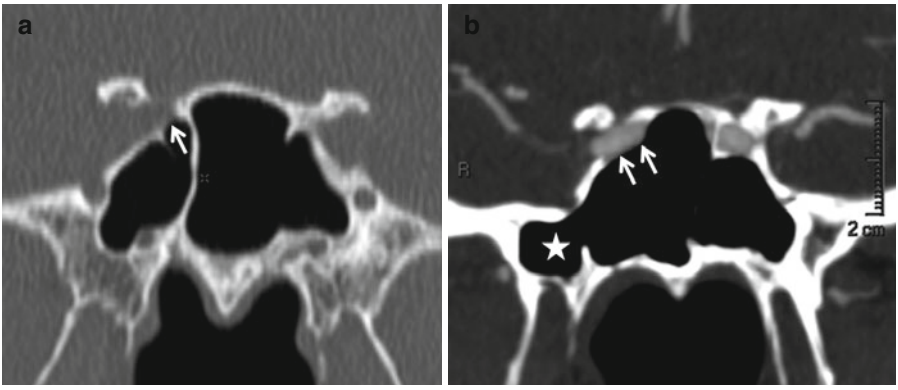

Fig. 9.9 The wall of the sphenoid sinus adjacent to the internal carotid arteries may be variable in thickness. In these images, there is no bony separation between the right ICA and the sinus cavity (*arrows*, **a** and **b**). In (**b**), note that pneumatization of the sphenoid sinus extends to the root of the pterygoid process (*asterisk*, pterygoid recess). A pterygoid recess may be the site of mucocele formation. Also, the greater sphenoid wing overlying, it can be thin enough to permit a CSF leak in some patients

Fig. 9.10 Alternating physiologic congestion and decongestion of the mucosa of the nasal cavity is known as the nasal cycle. Note that the mucosa of the right inferior turbinate is more prominent than on the left on this T2-weighted MR image. This must not be misconstrued as pathology

For effective evaluation using MRI, precontrast T1-weighted images must be obtained without fat suppression. The intrinsic T1 hyperintensity of fat provides a useful contrast against which low T1 signal intensity disease processes are easily seen. Fat suppression is useful on postcontrast T1-weighted sequences and enables the detection of enhancing abnormalities against a background of low fat signal. MRI is best used in mapping the extent of neoplasms and in the evaluation of intracranial spread of infectious diseases.

Plain radiography in the evaluation of sinonasal disease plays a minor role. One may rarely encounter a Waters' view of the paranasal sinuses, obtained to

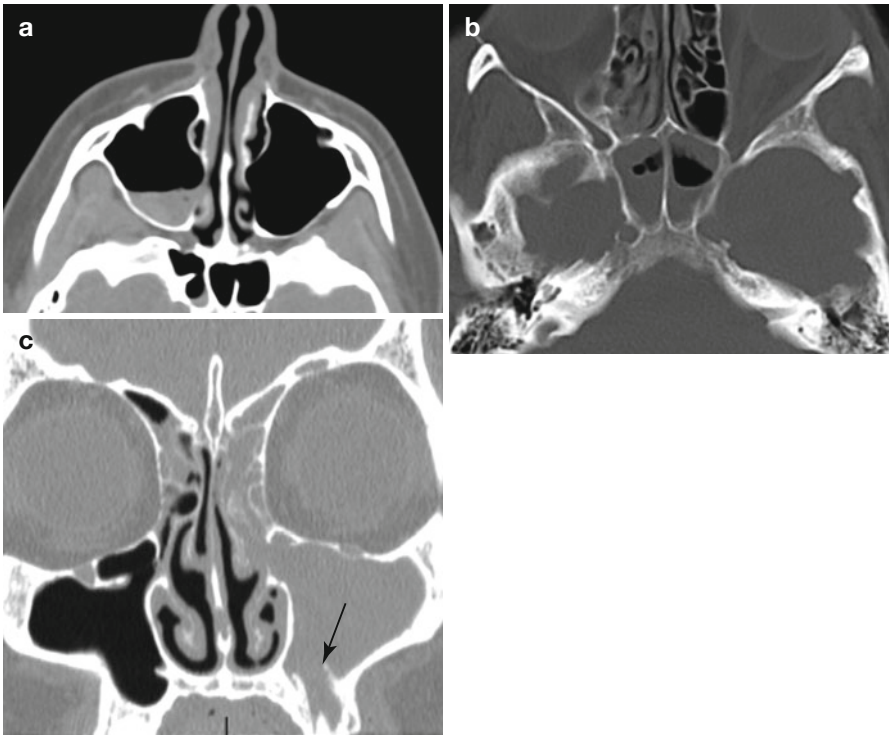

Fig. 9.11 Acute sinusitis. Fluid levels, in the appropriate clinical setting, indicate acute sinusitis (**a**, **b**). In a patient with acute maxillary sinusitis, it is always useful to evaluate the upper teeth. When periodontal disease occurs in a maxillary tooth whose roots project into the antrum, odontogenic sinusitis may occur (**c**, *arrow*)

demonstrate the presence of fluid/fluid levels in the setting of acute sinusitis. Plain films may also be used to evaluate nasal bone fractures, but ideally these are diagnosed clinically. Catheter angiography is best utilized for preoperative embolization of vascular sinonasal lesions such as juvenile nasopharyngeal angiofibromas and in the treatment of epistaxis.

9.3 Inflammatory Sinonasal Disease

9.3.1 Acute Inflammation and Its Complications

Acute inflammation of the sinuses may occur due to viral, bacterial, fungal, or allergic causes. A classic radiographic sign of acute sinusitis is a fluid level, but fluid levels may also be seen in a setting of trauma, prolonged nasogastric intubation, barotrauma, or CSF leak (Fig. 9.11). The presence of frothy secretions in a sinus may also indicate acute inflammation. Given the tendency of acute frontal and

Box 9.3. Complications of Acute Sinusitis

Orbital	
	Preseptal cellulitis
	Postseptal cellulitis
	Subperiosteal abscess
	Intraorbital abscess
	Cavernous sinus thrombophlebitis
Intracranial	
	Meningitis
	Subdural empyema
	Epidural abscess
	Cerebritis
	Brain abscess
	Dural sinus thrombosis
Others	
	Subpericranial abscess (Pott's puffy tumor)
	Calvarial/skull base osteomyelitis

sphenoid sinusitis to progress to life-threatening complications, it is imperative that the clinician be alerted to fluid levels in these areas. Acute sinusitis may also manifest as thickened mucosa on CT. The signs of early acute fungal sinusitis may be subtle and are discussed below.

Complications of acute sinusitis may involve the orbits or cranial cavity (Box 9.3). The orbits are most likely to be affected by ethmoid sinusitis. The lamina papyracea is a poor barrier to the spread of infection. The absence of valves in the anterior and posterior ethmoid veins also permits free spread of infection into the orbits. An extensive intradiploic anastomotic venous network allows spread of infection between the frontal sinuses and the meninges.

Orbital complications follow a loosely defined sequence of events (Fig. 9.12). Preseptal cellulitis (stage I) is manifested on CT by thickening and enhancement of the eyelid soft tissues; this can, however, be the consequence of simple transudative edema from impaired sinus venous outflow. At this stage, inflammation is restricted from posterior spread by the orbital septum. With orbital (postseptal) cellulitis (stage II), the intra- and extraconal fat demonstrates increased attenuation and stranding. The presence of a lentiform peripherally enhancing collection, applied to the lamina papyracea or orbital plate of the frontal bone and confined by the periorbita, indicates a subperiosteal abscess (stage III). A similar collection within the orbit itself indicates an orbital abscess (stage IV). Left untreated, this progresses to thrombophlebitis of the superior and inferior ophthalmic veins and then of the cavernous sinus itself (stage V). Enlargement and lack of enhancement of these venous structures, a convex contour to the cavernous sinus, and extraocular muscle engorgement are signs of cavernous sinus thrombosis. While unenhanced MRI may show T1 hyperintense thrombus in the cavernous sinus, contrast-enhanced CT or MRI is

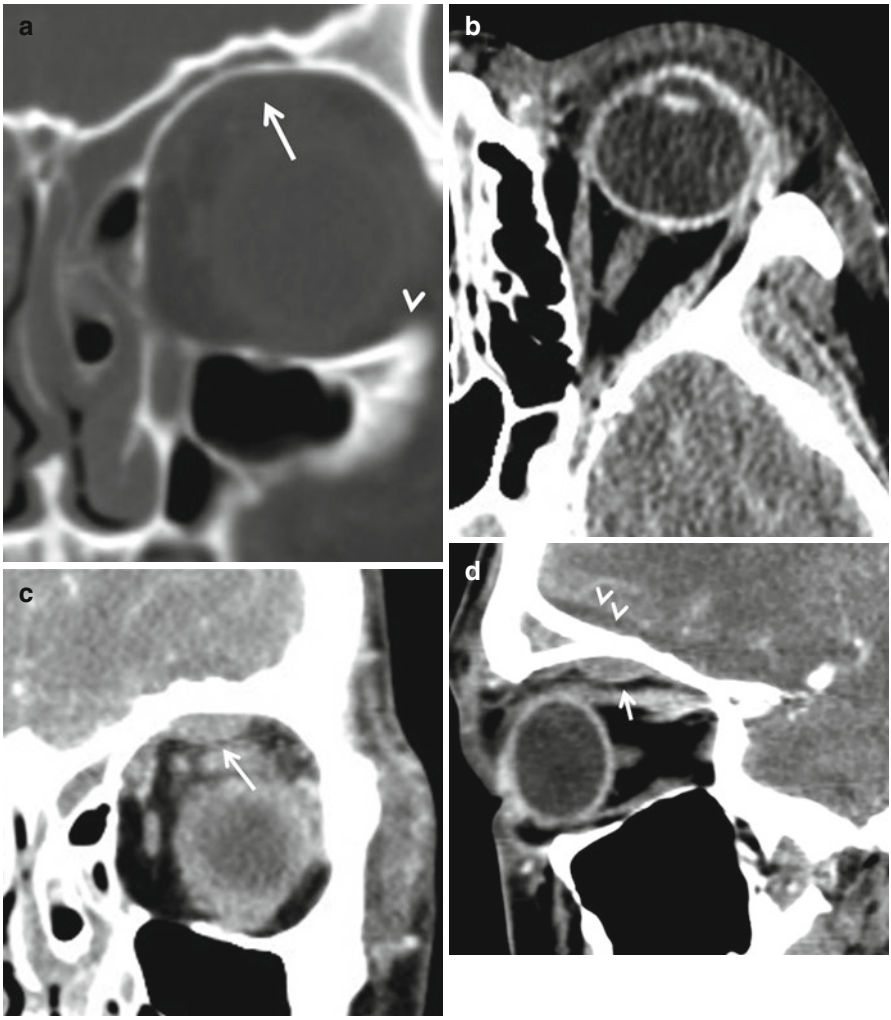

Fig. 9.12 (**a**) Orbital complications of acute frontal and ethmoid sinusitis. Image (**a**) shows fluid in the frontal and ethmoid air cells. In (**b**), edema of the preseptal soft tissues (*arrows*) is evident. The *white lines* roughly indicate the plane of the orbital septum, a fibrous sheet that is an effective but not always reliable barrier to the spread of inflammation. In (**c**, **d**), a lentiform collection (*arrows*) with its base against the orbital roof representing a subperiosteal abscess is present. Also in (d), note a low-density epidural abscess (*arrowheads*) under the right frontal lobe. Inspecting CT images in narrow window settings may help detect subtle findings of intracranial complications. In (**e**), on this contrast-enhanced fat-suppressed MR image, the epidural abscess and the associated meningeal enhancement (*arrowhead*) are obvious. Also, note the stranding and enhancement of the orbital fat (*asterisk*) indicating cellulitis and thickening and enhancement of the superior rectus and oblique muscles representing myositis (*arrows*). Diffusion-weighted images are very useful in demonstrating intracranial purulence (*arrows*, **f**). The graphic, (**g**), illustrates the various complications that may follow acute bacterial sinusitis – preseptal cellulitis (*double arrows*), postseptal cellulitis, subperiosteal abscess (*black asterisk*), meningitis (*arrowheads*), intracranial empyema (*white asterisk*), and cavernous sinus thrombosis (*white arrow*)

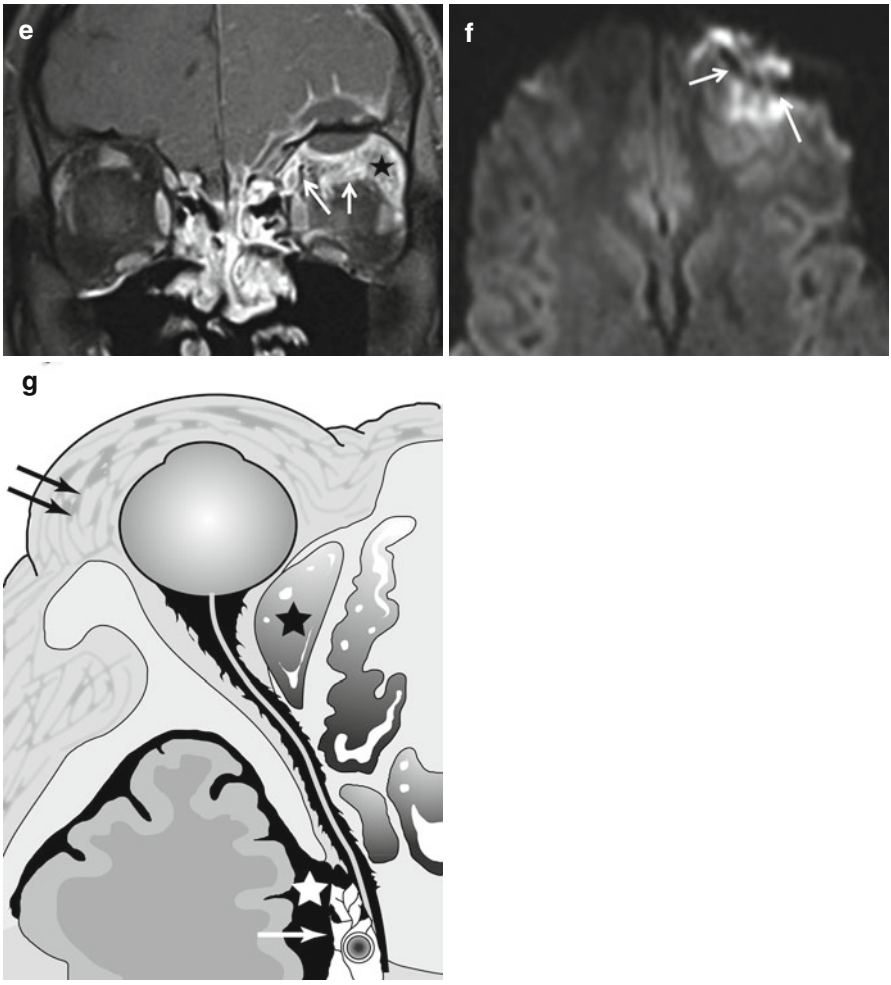

Fig. 9.12 (continued)

the best imaging modality to evaluate this entity. MR venography is usually insensitive to cavernous sinus thrombosis as the normal cavernous sinuses themselves are not well seen.

The intracranial complications of sinusitis are best evaluated by MRI (Fig. 9.13). However, when presented with a CT, it is useful to examine the brain and extra-axial spaces in narrow window settings to detect subtle abnormalities such as small subdural or epidural infectious collections. Meningitis is recognized on MRI by increased signal intensity in the subarachnoid spaces on FLAIR imaging and by leptomeningeal enhancement with administration of contrast. Diffusion-weighted imaging (DWI) is useful in the detection of extra-axial empyemas, which appear

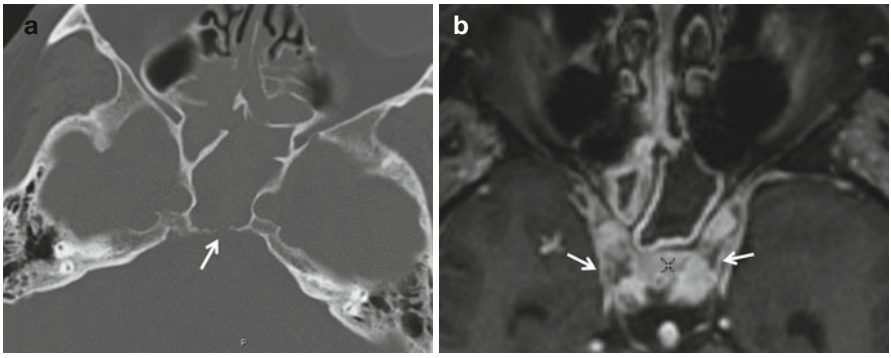

Fig. 9.13 (**a**) Bacterial sphenoid sinusitis with cavernous sinus thrombosis. Note the focus of bone destruction in (a) (*arrows*). This patient presented with fever and headache rapidly followed by chemosis and ophthalmoplegia. In (**b**), the filling defects in the cavernous sinuses bilaterally represent thrombi. Cavernous sinus thrombosis is best depicted on contrast-enhanced MR images (*arrows*). MR venography is not useful because the normal cavernous sinuses are not well depicted on this modality

hyperintense. Sterile effusions are not hyperintense on DWI. Pyogenic brain abscesses are also characteristically hyperintense on DWI. Vascular complications such as dural venous sinus thrombosis and mycotic ICA pseudoaneurysms are best demonstrated by MR venography and angiography, respectively.

9.3.2 Fungal Sinusitis

Fungal sinusitis manifest in four different forms: allergic fungal sinusitis, noninvasive fungal sinus colonization (mycetoma), acute invasive fungal sinusitis, and chronic invasive fungal sinusitis. Of these, allergic fungal sinusitis is the commonest and occurs as a result of an IgE-mediated hypersensitivity response to fungal antigens. It is usually caused by fungi of the *Fusaria*, *Bipolaris*, and *Aspergillus* species, among others. Affected sinuses contain inspissated mucin which gradually accumulates, expands, and thins bony sinus walls. Commonly, all the sinuses and the nasal cavity are simultaneously affected (Fig. 9.14). The mucin contains concentrated protein and fungal elements and heavy metals such as iron and manganese, resulting in hyperdensity on CT and low signal on T1- and T2-weighted MRI, a finding that may simulate a pneumatized sinus. On gadolinium MRI, the mucosa enhances while the sinus contents do not, enabling differentiation from neoplasm. Sinus wall expansion leads to gradual demineralization and erosion, and extension of the disease into the orbits and cranial cavity may follow. A mycetoma results from colonization of a chronically inflamed sinus, usually the maxillary, and appears as a calcified mass on CT. An irregular, calcified mass within a chronically inflamed sinus is almost always a mycetoma (Fig. 9.15).

Acute invasive fungal sinusitis usually occurs in immunocompromised patients. Imaging findings can be exceedingly subtle and must be actively sought in the context of immunosuppression (Fig. 9.16). The culprit fungi are usually *Rhizopus*,

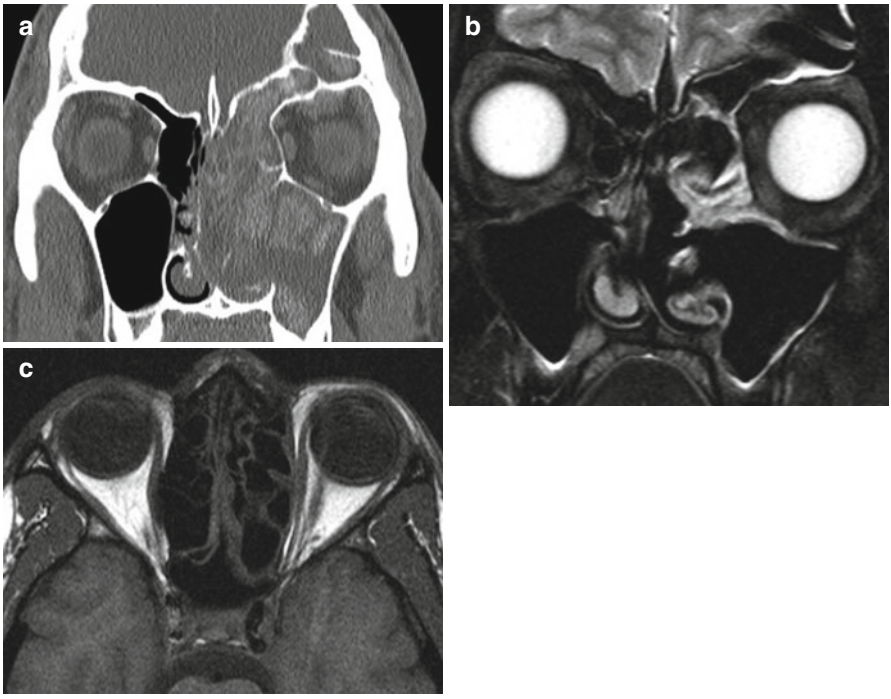

Fig. 9.14 Allergic fungal sinusitis. The hyperdense appearance of the inspissated secretions in the left frontal ethmoid and maxillary sinuses is typical of this entity (**a**). It is not uncommon for the sinuses to be expanded as in this case. It is important to note that in (**b**, **c**), T2- and T1-weighted images, the complete absence of signal in the involved sinuses is not indicative of absence of disease but is a consequence of the extremely high protein and heavy metal concentrations in the secretions

Mucorales, *Absidia*, and *Mucor*. They are angioinvasive and can thus erode the sinus walls and access the orbits and intracranial compartment even in the presence of only minimal sinus imaging findings. The bony changes are best seen on CT while intracranial and orbital spread is best assessed by MRI. Abnormal soft tissue in the retroantral, extraconal, orbital apex, and pterygopalatine fossa (PPF) fat may indicate spread beyond the sinus. The precontrast T1-weighted images are especially useful in evaluating these regions which should show hyperintense fat signal if normal. The flow voids of the cavernous ICA must also be carefully inspected; thrombosis and pseudoaneurysm can occur as a complication of invasive fungal sinusitis. The black turbinate sign, which reflects non-enhancing, ischemic middle turbinate mucosa, may be an early indicator of invasive sinusitis. Fungi may also spread along preexisting canals and foramina, which may simulate perineural tumor spread.

Chronic invasive fungal sinusitis follows a more indolent course and can occur in immunocompetent patients as well. A combination of sinus opacification, bone destruction, and extra-sinus soft tissue is typical. These findings can mimic malignant neoplasms or other entities such as sarcoidosis and Wegener's

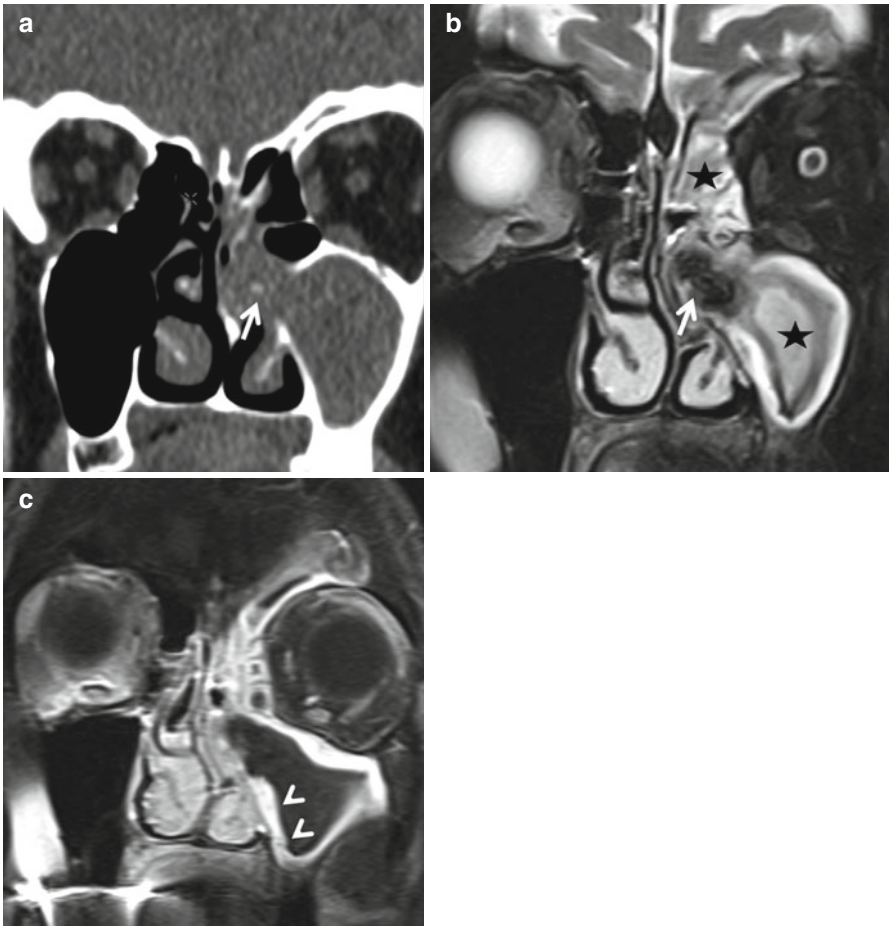

Fig. 9.15 Mycetoma. The CT demonstrates expansion of the left infundibulum by a soft tissue lesion containing foci of calcification (*arrow*, **a**). In (**b**), A T2W image, the infundibular lesion is of low signal intensity. It does not enhance with gadolinium in (**c**). These findings are typical for a mycetoma. The *asterisks* in (b) indicate fluid in the obstructed maxillary and ethmoid air cells. The *arrowheads* in (c) point to enhancement of the edematous sinus mucosa. A pattern of unilateral ostiomeatal unit disease in an adult must always prompt close scrutiny of the middle meatus for an obstructing mass lesion

granulomatosis, and definitive diagnosis may not be possible with imaging alone.

9.3.3 Chronic Rhinosinusitis (CRS)

CRS is manifested by any combination of polyps, retention cysts, sinus wall osteitis, and mucocele formation. The role of anatomic variations such as conchae bullosa, paradoxical turbinates, Haller cells, and pneumatized uncinate processes in

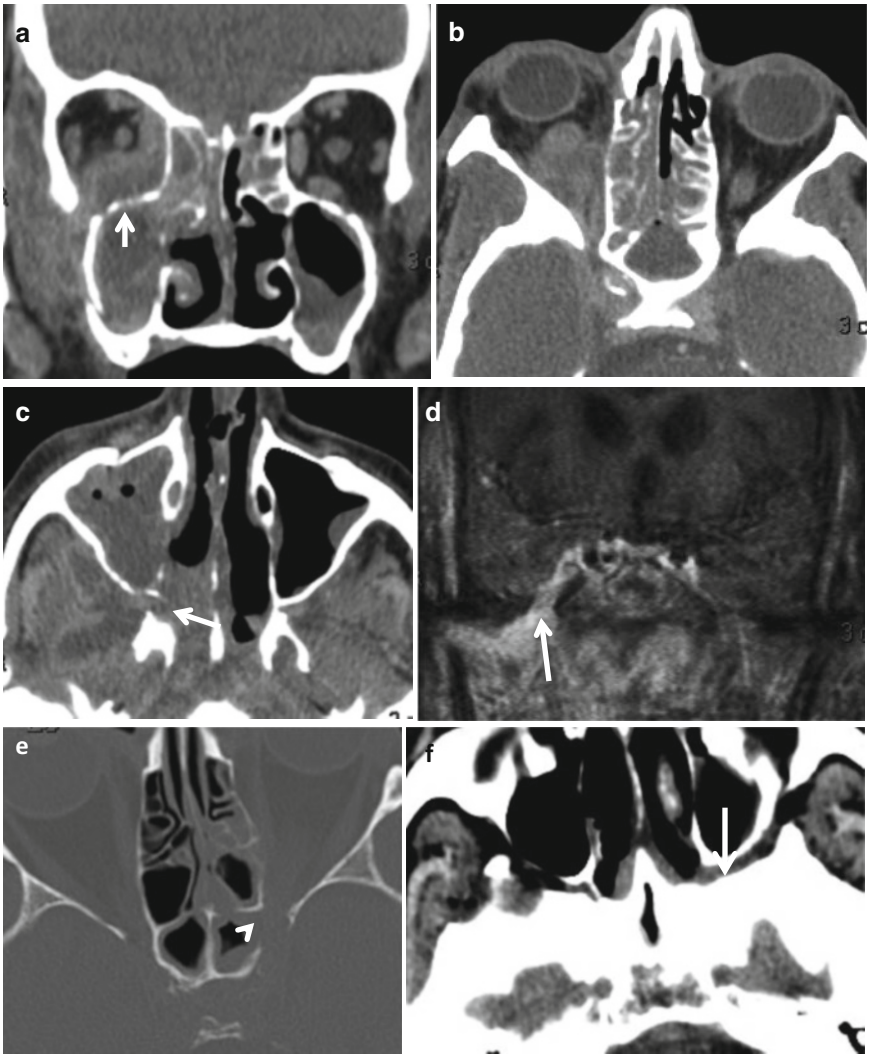

Fig. 9.16 Invasive fungal sinusitis. Images (**a**–**d**) are from a patient with diabetes mellitus and invasive Aspergillus sinusitis. Fungal sinusitis can rapidly spread from the sinonasal cavities to the orbits (**b**) and skull base as in this case. Note the permeative bone destruction of the maxillary sinus wall in (a) (*arrow*), a finding typical of this entity. The inflammatory process can also spread along pathways of least resistance such as the pterygopalatine fossa (*arrow* **c**) and skull base foramina (*arrow*, foramen ovale, **d**) to gain access to the cranial cavity. The sinus inflammation in invasive fungal sinusitis may not be impressive, as in (**e**), where a small amount of ethmoid and sphenoid mucosal thickening is associated with destruction of the wall of the sinus adjacent to the optic canal (*arrowhead*). Spread of infection beyond the sinus and orbits is evident in the left pterygopalatine fossa where the normal fat is replaced by soft tissue (*arrow*, **f**). Images (**g**, **h**) are from a patient with invasive aspergillosis who presented with a sixth nerve palsy. The mucosal inflammation in the sphenoid sinus is not impressive, but the fat-suppressed axial T1-weighted MR image reveals enhancement of the clival and left petrous apex marrow (*arrows*) and of the dura (*arrowheads*) along the posterior aspect of the petrous bone

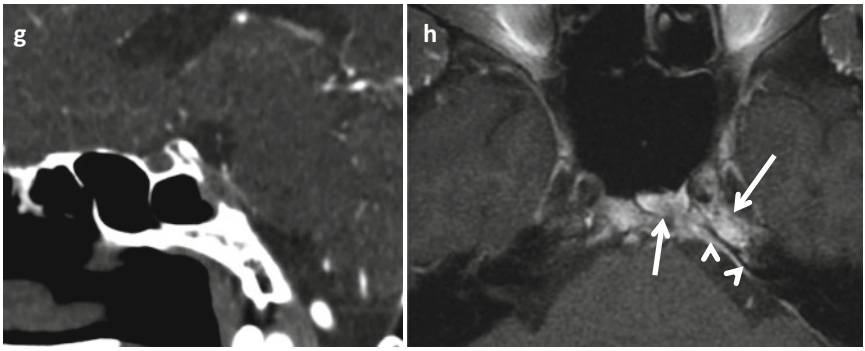

Fig. 9.16 (continued)

predisposing to CRS is debatable. Deviation of the nasal septum and a horizontal orientation of the uncinate process may be more frequent in patients with CRS.

Polyps and mucosal retention cysts are distinct histologically but indistinguishable on noncontrast CT imaging. They are most often seen as incidental findings and are usually of no clinical significance. Polyps may be solitary or numerous and can vary greatly in size. Occasionally a large polyp arising from the maxillary sinus can protrude into the nasal cavity through the maxillary ostium (antrochoanal polyp). Polyps on CT may be indistinguishable from tumors such as inverted papillomas, melanomas, and lymphomas. The presence of smooth remodeling of adjacent bone and internal hyperdensities suggests a benign diagnosis. The hyperdensity is due to the presence of inspissated secretions or fungal colonization. On contrast-enhanced MRI, polyps enhance peripherally while tumors are more likely to enhance in a solid fashion. On MRI, polyps and the fluid collected between them can demonstrate complex signal intensities. Retained sinus secretions demonstrate progressive increase in protein concentration. As protein concentration increases, T1-weighted signal intensity also increases. T1 hyperintensity is usually reassuring for benign disease, with the exception of melanotic melanoma. With very high protein concentrations, T1 signal intensity declines. T2 signal intensity declines with increasing protein concentration and, when protein concentrations exceed 35–40 %, signal may disappear entirely, giving rise to a signal void, which may appear as a falsely aerated sinus (Fig. 9.14).

Chronically inflamed sinuses provoke inflammatory osteitis in the sinus walls that manifests as bone thickening, easily seen on CT (Fig. 9.17). Obstruction of the sinus ostium can result in the formation of a mucocele, which requires expansion of the sinus. Mucoceles (Fig. 9.18) may also arise as a consequence of previous trauma or surgery. The frontal and anterior ethmoid sinuses have relatively small ostia and are more likely to form mucoceles, which can become symptomatic due to extension into the orbits or cranial cavity. Intraorbital extension is more likely to occur with frontal and ethmoid mucoceles. The rare sphenoid mucocele can encroach upon the orbital apex. Mucoceles may also become secondarily infected (mucopyocele) and, in the frontal sinus, give rise to "Pott's puffy tumor," a purulent subpericranial fluid collection (Fig. 9.19).

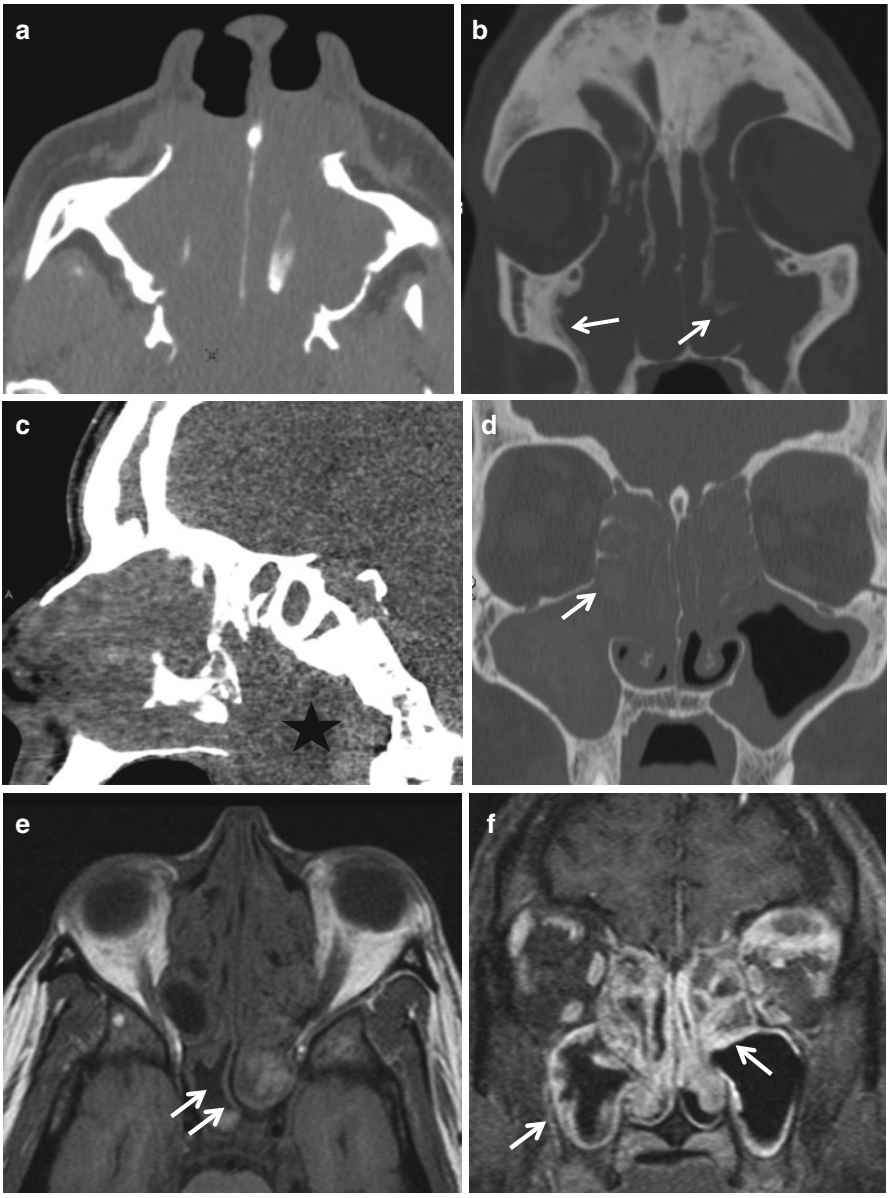

Fig. 9.17 Sinonasal polyposis. Images (**a**–**c**) demonstrate complete opacification of the nasal cavity and paranasal sinuses by diffuse polyposis. Note the extensive demineralization of the ethmoid septa, medial antral walls, and the turbinates in (**a**, **b**). Foci of sclerosis (*arrows*, **b**) are due to chronic osteitis. In (**c**), a large antrochoanal polyp obstructing the posterior choana is noted (*asterisk*). Similar findings are seen in images (**d**) in a patient with long-standing allergic rhinosinusitis. The presence of hyperdense foci and peripheral mucosal enhancement (*arrows* in **d**, **f** respectively) is typical for polyposis. Note trapped secretions of varying signal intensities produced by differing protein concentrations on the unenhanced T1-weighted image (*arrows*, **e**)

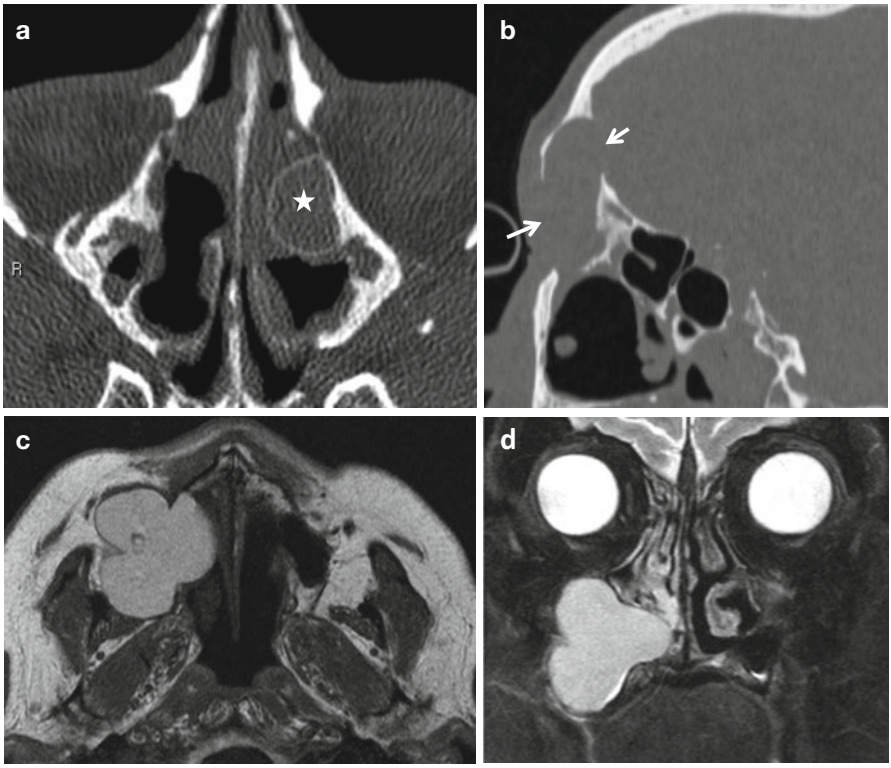

Fig. 9.18 Mucoceles. A mucocele is an obstructed fluid-filled expanded sinus. (**a**) Shows a left anterior ethmoid air cell mucocele (*asterisk*) in a patient with persistent symptoms after sinus surgery. It is not unusual for the wall of large mucoceles to become extremely attenuated as in the case of the frontal mucocele in (**b**) (*arrows*). A maxillary mucocele is shown in (**c**, **d**). The contents of mucoceles on MR are often T1 hyperintense due to their proteinaceous nature

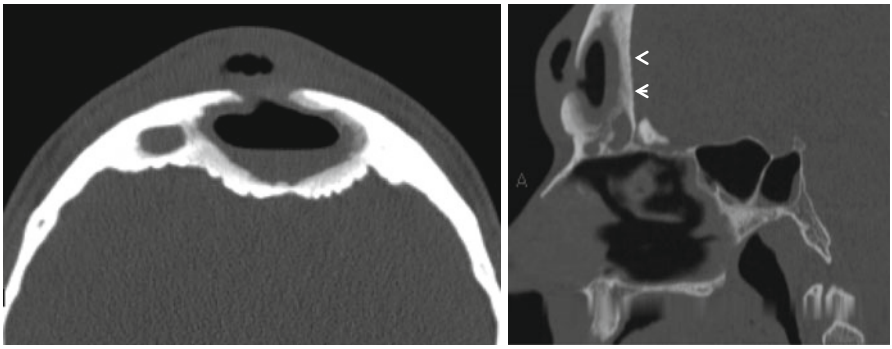

Fig. 9.19 Pott's puffy tumor is the term applied to a collection of pus under the frontal pericranium arising from a frontal sinus mucopyocele. Note the expansion of the frontal sinus, the fluid level, and the chronic osteitis of the frontal sinus walls (*arrowheads*)

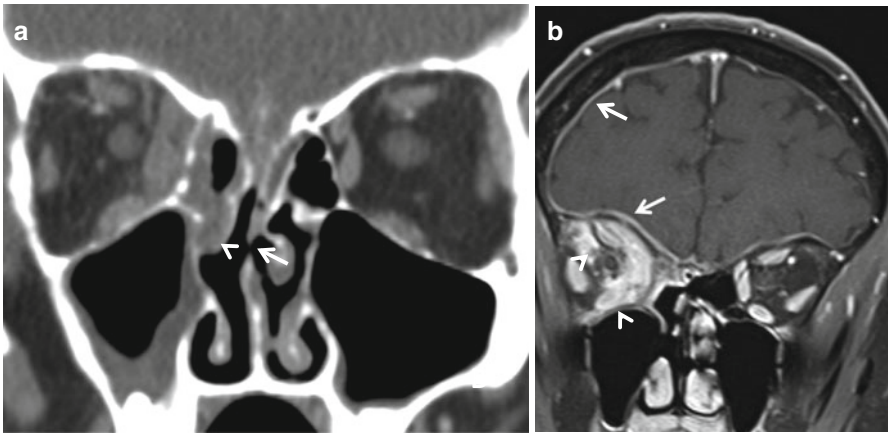

Fig. 9.20 Wegener's granulomatosis. The imaging findings in WG are often indistinguishable from nonspecific chronic rhinosinusitis. However involvement of the nasal septum (*arrow*, **a**) and erosive changes as in the case of the right middle turbinate (*arrowhead* **a**) are highly suggestive of the diagnosis, especially if orbital and meningeal involvements (*arrowheads* and *arrows*, respectively, in **b**) are present

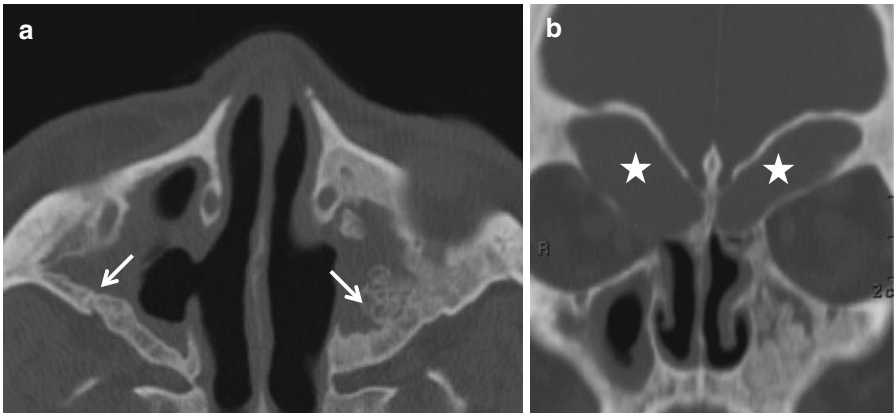

Fig. 9.21 Sarcoidosis. Imaging findings in sinonasal sarcoidosis are nonspecific, reflect long-standing sinus inflammation, and may sometimes resemble those in Wegener's granulomatosis in terms of a tendency to affect the nasal septum and coexistence of orbital and intracranial disease. In this case florid sclerosis of the sinus walls due to chronic osteitis (*arrows*, **a**) and bilateral frontal mucoceles (*asterisks*, **b**) is present

9.3.4 Noninfectious Inflammatory Conditions

The imaging appearance of Wegener's granulomatosis is extremely variable (Fig. 9.20). The diagnosis may be suspected based on involvement of the nasal septum, the presence of soft tissue masses within the sinus cavities, bone sclerosis, and extension into the adjacent soft tissues and the orbits. Sarcoidosis can also affect the sinonasal cavity and presence of any combination of mucosal thickening, bone destruction, soft tissue masses, and extension beyond the sinuses (Fig. 9.21).

A chronic smoldering inflammatory sinonasal process in an African American patient may indicate sarcoidosis. Ultimately, the overall clinical picture and nasal biopsy are crucial in making the final diagnosis. Another more rare diagnostic consideration in the presence of these imaging findings would be inflammatory pseudotumor (IPT), an idiopathic entity of autoimmune/infectious etiology. Perhaps due to the presence of a fibrous component, IPT may appear hypointense on T2-weighted imaging (Fig. 9.22).

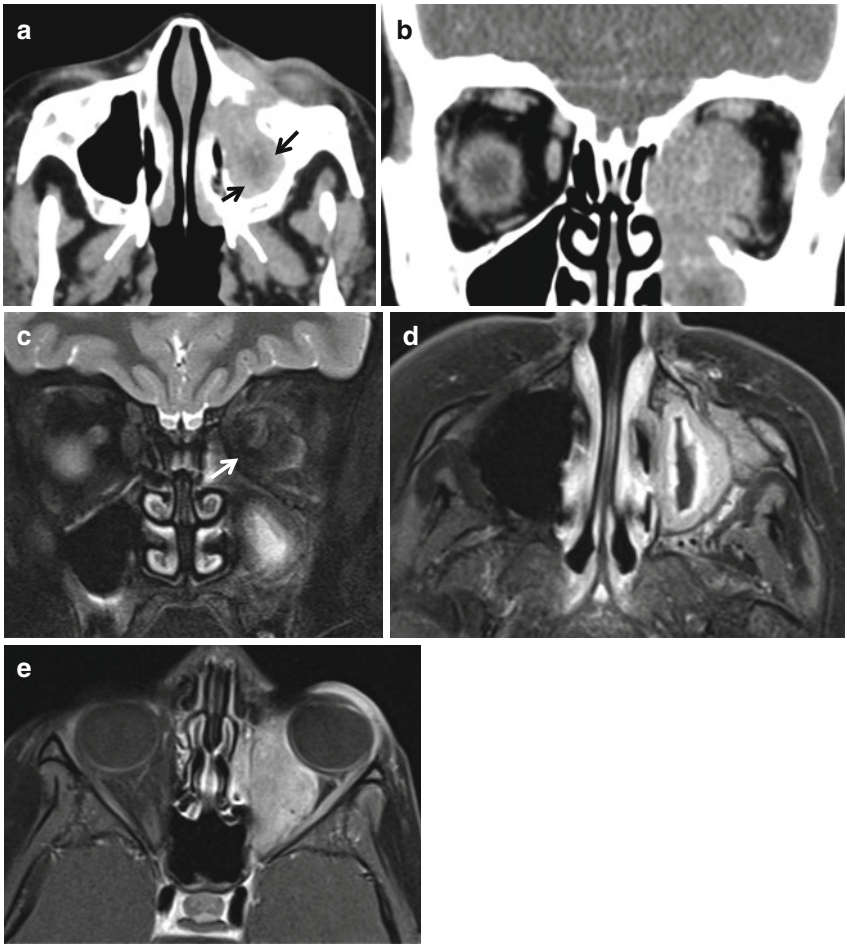

Fig. 9.22 Sino-orbital inflammatory pseudotumor. A thick rind of enhancing soft tissue (*arrows*) is seen in the left maxillary antrum (**a**). It has extended into the left orbit where the medial rectus and superior oblique are engulfed and the intraconal fat invaded (**b**). On the T2-weighted image (**c**), the lesion is profoundly hypointense (*arrow*), a finding that is strongly suggestive of IPT. The contrast-enhanced images (**d**, **e**) reveal fairly intense enhancement. Biopsy revealed IgG4-positive IPT, an entity associated with elevated serum IgG4 which can affect other structures such as the pancreas, salivary glands, thyroid, lungs, pleura, and retroperitoneum among others

9.4 Sinonasal Neoplasms

9.4.1 Malignant Neoplasms

A brief classification of malignant sinonasal tumors is provided in Box 9.4. Although most sinonasal malignant tumors have no characteristic imaging appearance, esthesioneuroblastoma (olfactory neuroblastoma) can occasionally be identified by cysts capping the superior portion of the tumor, and some melanomas are hyperintense on T1-weighted imaging due to a combination of melanin and hemorrhage (Fig. 9.23).

Squamous cell carcinoma is the most common malignant sinonasal tumor; a simplified staging system is provided in Box 9.5. Esthesioneuroblastoma is commonly staged by the Kadish system, with stage A representing tumors confined to the nasal cavity, stage B signifying extension into the paranasal sinuses, and stage C indicating orbital or intracranial extension. A TNM system is also used for esthesioneuroblastoma staging (Box 9.6). The radiologist's primary role is to determine resectability, which requires addressing the following questions:

1. Is there orbital invasion?
2. Is there invasion of the dura or brain parenchyma?
3. Is there perineural tumor spread?
4. Is there skull base invasion?

Box 9.4. Malignant Sinonasal Tumors

- Epithelial origin
  - Squamous cell carcinoma
  - Intestinal type adenocarcinoma
  - Malignant minor salivary gland tumors
    - Adenoid cystic carcinoma
    - Mucoepidermoid carcinoma
- Neuroectodermal origin
  - Esthesioneuroblastoma
  - Sinonasal undifferentiated and neuroendocrine carcinoma
  - Melanoma
- Mesenchymal origin
  - Osteosarcoma
  - Chondrosarcoma
  - Ewing's sarcoma
  - Malignant nerve sheath tumor
  - Rhabdomyosarcoma
  - Fibrosarcoma and malignant fibrous histiocytoma
  - Angiosarcoma
- Lymphoid malignancies
- Metastases

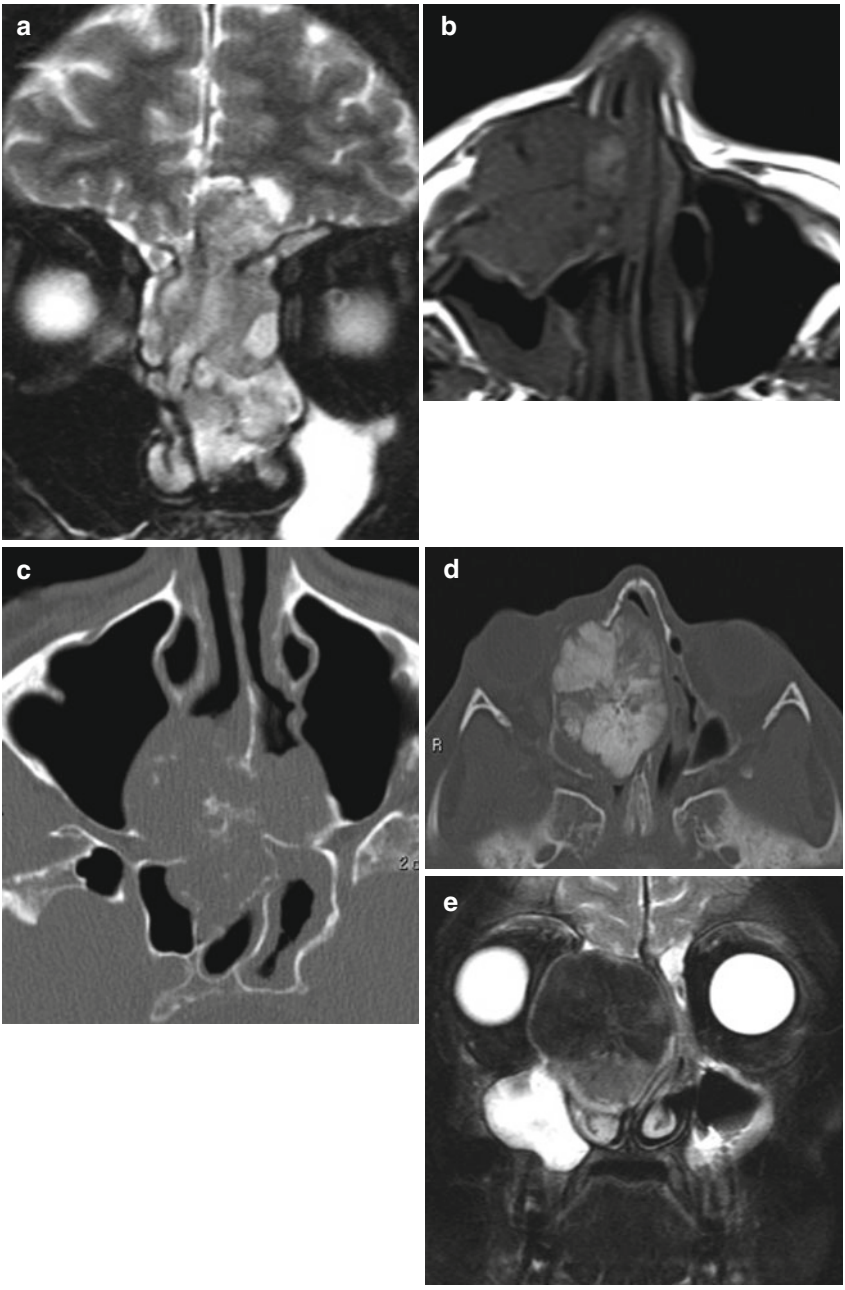

Fig. 9.23 Malignant sinonasal tumors. Sinonasal malignancies rarely demonstrate defining imaging characteristics. However, the presence of cysts capping the intracranial portion of a tumor (**a**) may be a sign of an esthesioneuroblastoma. Areas of T1 hyperintensity due to melanin or hemorrhage (*arrow*, **b**) may be seen with melanomas. Image (**c**) shows arc and whorl-like calcifications, a finding when present is highly suggestive of chondrosarcoma. In (**d**, **e**), a sunburst pattern of tumor bone formation, characteristic of osteosarcoma, is present

Box 9.5. TNM Staging of Nasal Cavity, Maxillary, and Ethmoid Sinus Squamous Cell Carcinoma

TX	Primary tumor cannot be assessed
T0	No evidence of primary tumor
Tis	Carcinoma in situ
Maxillary sinus	
T1	Tumor limited to maxillary sinus mucosa
T2	Tumor causing bone erosion or destruction including extension into the hard palate and/or middle nasal meatus, except extension to posterior wall of maxillary sinus and pterygoid plates
T3	Tumor invading any of the following: posterior wall of maxillary sinus, subcutaneous tissues, floor or medial wall of orbit, pterygoid fossa, or ethmoid sinuses
T4a	Moderately advanced local disease Tumor invades anterior orbital contents, skin of cheek, pterygoid plates, infratemporal fossa, cribriform plate, or sphenoid or frontal sinuses
T4b	Very advanced local disease Tumor invades any of the following: orbital apex, dura, brain, middle cranial fossa, cranial nerves other than maxillary division of trigeminal nerve (V_2), nasopharynx, or clivus
Nasal cavity and ethmoid sinus	
T1	Tumor restricted to any one subsite, with or without bony invasion
T2	Tumor invading two subsites in a single region or extending to involve an adjacent region within the nasoethmoidal complex, with or without bony invasion
T3	Tumor extends to invade the medial wall or floor of the orbit, maxillary sinus, palate, or cribriform plate
T4a	Moderately advanced local disease Tumor invades any of the following: anterior orbital contents, skin of nose or cheek, minimal extension to anterior cranial fossa, pterygoid plates, or sphenoid or frontal sinuses
T4b	Very advanced local disease Tumor invades any of the following: orbital apex, dura, brain, middle cranial fossa, cranial nerves other than (V_2), nasopharynx, or clivus
Regional lymph nodes (*N*)	
NX	Regional lymph nodes cannot be assessed
N0	No regional lymph node metastasis
N1	Metastasis in a single ipsilateral lymph node, ≤3 cm in greatest dimension
N2	Metastasis in a single ipsilateral lymph node, >3 cm but ≤6 cm in greatest dimension, or metastases in multiple ipsilateral lymph nodes, ≤6 cm in greatest dimension, or in bilateral or contralateral lymph nodes, ≤6 cm in greatest dimension
N2a	Metastasis in a single ipsilateral lymph node, >3 cm but ≤6 cm in greatest dimension
N2b	Metastases in multiple ipsilateral lymph nodes, ≤6 cm in greatest dimension
N2c	Metastases in bilateral or contralateral lymph nodes, ≤6 cm in greatest dimension
N3	Metastasis in a lymph node, >6 cm in greatest dimension
Distant metastasis (*M*)	
M0	No distant metastasis
M1	Distant metastasis

Reprinted with permission from AJCC: paranasal sinus and nasal cavity. In: Edge SB, Byrd DR, Compton CC et al (eds) (2010) AJCC cancer staging manual, 7th edn. Springer, New York, p 69–78

These questions are best answered by a combination of CT and MRI. CT is useful to detect destruction of the cribriform plates, fovea ethmoidalis, pterygoid plates, and lamina papyracea. MRI is best used to identify orbital, skull base, and perineural invasion. MRI is also useful in enabling distinction between tumor and obstructed secretions and mucosal inflammation. Given its resistance to tumor spread, the orbit is only considered invaded when the periorbita is breached; when this has occurred, the globe is usually not salvageable. The only reliable sign of orbital invasion is engulfment of one or more extraocular muscles by tumor. While other signs have been described, such as irregular tumor margins, loss of the fat plane between the tumor and the extraocular musculature, and abnormal muscle signal intensity and enhancement, these are unreliable (Fig. 9.24).

Dural invasion may be difficult to determine. Enhancement of the dura can be reactive to tumor; such enhancement is linear and usually less than 5 mm thick. Any nodularity of enhancement or enhancement of the adjacent leptomeninges must be interpreted as meningeal invasion. The presence of parenchymal edema is usually a sign of frank brain invasion (Fig. 9.25).

Perineural tumor spread may occur with any malignancy but is especially common with adenoid cystic carcinoma. The close proximity of the PPF to the sinonasal cavities means that a tumor that invades the PPF has easy access to the skull base. The PPF contains predominantly fat, which is easily seen on CT or on T1-weighted sequences; loss of this fat is always worrisome. Perineural spread may occur in any direction from the PPF and can present as skip lesions. It is therefore important to scrutinize the PPF and all its associated foramina when evaluating a sinonasal malignancy. CT is not very sensitive in the detection of perineural tumor spread, but widening of skull base foramina and loss of the PPF fat can be appreciated. MRI is the best way to evaluate perineural spread using a combination of the precontrast nonfat-suppressed T1-weighted and postcontrast fat-suppressed T1-weighted imaging. Involved nerves are thickened and enhance abnormally (Fig. 9.26).

The skull base is best evaluated with a combination of CT and MRI. The normal skull base marrow is fatty and therefore hyperintense on T1. Replacement of the fatty marrow may indicate tumor invasion, but hematological processes, osteoporosis, chronic smoking, and infection may also produce abnormal marrow signal. A combination of bone erosion on CT and abnormal marrow signal on MRI is the best evidence for skull base invasion.

9.4.2 Benign Neoplasms

The most common benign tumors are osteomas, fibro-osseous lesions, inverted papillomas, and juvenile angiofibromas. Osteomas appear as well-defined radiodense lesions on CT (Fig. 9.27). Multiple osteomas must make one suspect Gardner's syndrome, where there is an increased incidence of sebaceous cysts, extra-abdominal desmoid tumors, and thyroid, breast, and uterine malignancy (Fig. 9.27). Fibrous dysplasia and ossifying fibroma have similar imaging appearances. On plain films and CT, both can demonstrate bone expansion and a ground glass matrix. Ossifying fibromas tend to be less radiodense than fibrosis dysplasia and are usually better

circumscribed. Because they share common imaging features, the term "fibro-osseous lesion" may be used to refer to both. These lesions can demonstrate bizarre signal intensities and enhancement on MRI and can thus appear quite aggressive, which can be erroneously interpreted as malignancy (Fig. 9.28).

Juvenile angiofibromas (Fig. 9.29) are highly vascular tumors and occur exclusively in adolescent males. They originate at the sphenopalatine foramen and have a propensity to infiltrate the PPF, the skull base, and the orbits. Intense enhancement is characteristic on CT and MRI. Flow voids, representing feeding arteries or draining veins, may be seen on MRI. The vascular supply of angiofibromas is from the internal maxillary and ascending pharyngeal arteries, and preoperative embolization is common practice. It is important to note that in older individuals,

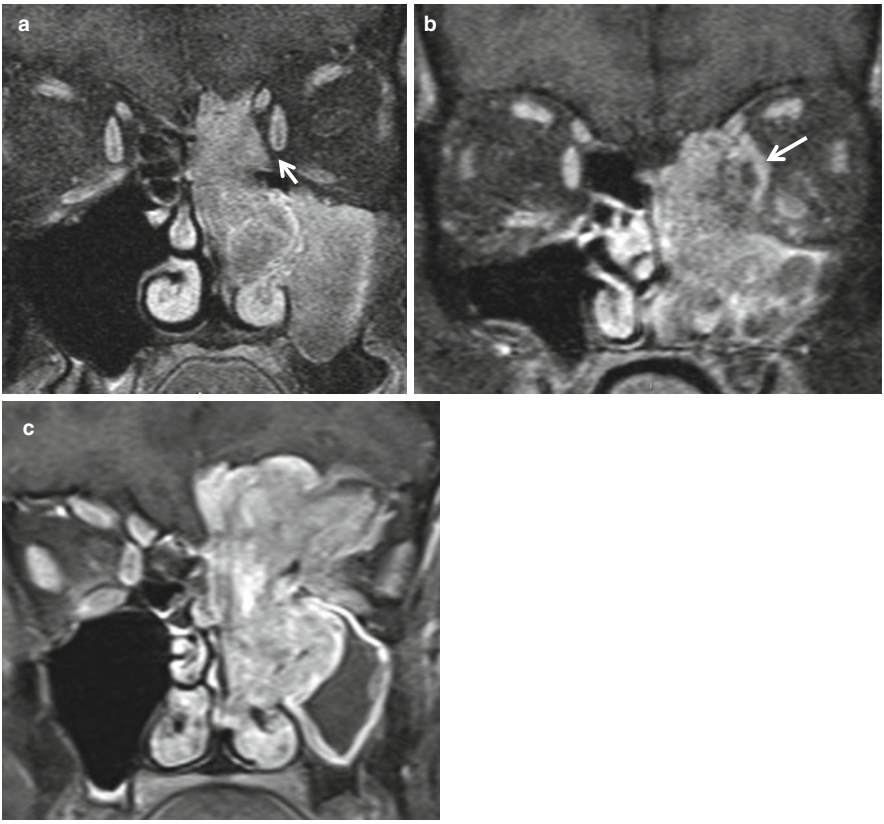

Fig. 9.24 The orbits in sinonasal malignancy. Three different patients with ethmoidal squamous cell carcinoma. In (**a**), a distinct fat plane (*arrow*) is visible between the tumor and the medial rectus indicating that the periorbita is intact and that the orbit is not violated. In (**b**), no fat plane is visible and the tumor displaces the medial rectus (*arrow*). This finding is equivocal for orbital invasion. At surgery, the periorbita was intact. In (**c**), violation of the periorbita is indicated by engulfment of the medial rectus and superior oblique muscles by tumor. It is important to note that destruction of the bony orbital walls does not indicate orbital invasion and that it is violation of the periorbita, a structure not seen on imaging that makes the globe unsalvageable. The graphic, (**d**), illustrates invasion of the periorbita on the right and its displacement on the left

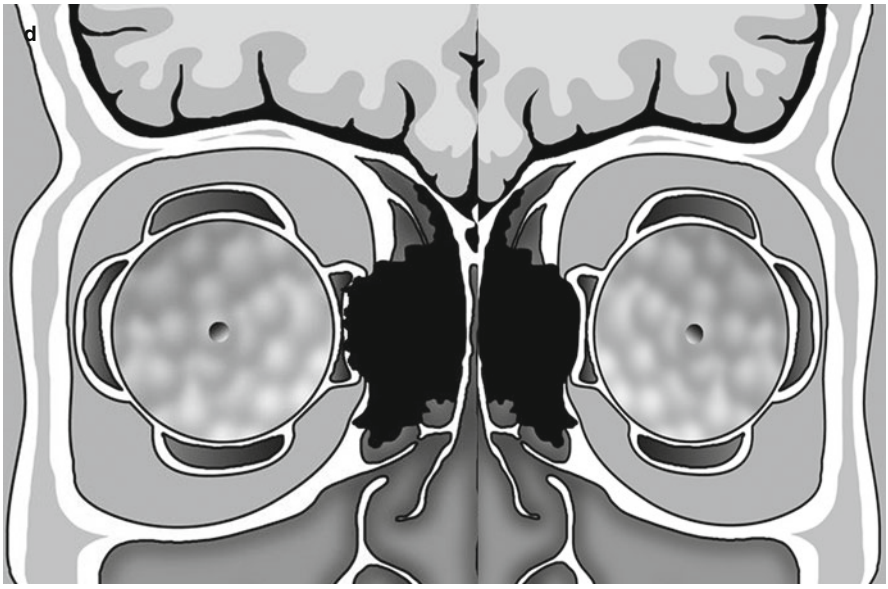

Fig. 9.24 (continued)

angiofibromas may involute spontaneously and, when imaged in the process of doing so, enhancement may not be as intense as expected. The angiomatous polyp is an entity that may appear similar to angiofibromas but does not enhance to the same extent or infiltrate to the same degree as angiofibromas do.

Three types of papillomas arise from the Schneiderian epithelium of the nasal cavity: inverted, fungiform, and cylindrical. Inverted papillomas arise from the lateral nasal walls near the middle turbinate and demonstrate an endophytic pattern of growth into the ethmoid and maxillary sinuses. Due to squamous metaplasia in the adjacent epithelium, inverted papillomas are associated with an increased risk of squamous cell carcinoma and should be removed with clear margins. On CT, inverted papillomas appear as lobulated masses containing fragments of destroyed bone. A focus of sclerosis in the lateral nasal wall may suggest the attachment site. The presence of bone destruction in association with an inverted papilloma is a worrisome sign and may indicate coexisting squamous cell carcinoma. On MRI, an inverted papilloma may demonstrate a convoluted so-called cerebriform appearance on postcontrast images (Fig. 9.30).

9.5 The Surgeon's Perspective

9.5.1 FESS

The mainstay of treatment for both acute and chronic sinusitis is medical. When considering a patient for functional endoscopic sinus surgery (FESS), imaging should be obtained at the point of maximal therapeutic benefit. Functional endoscopic sinus surgery (FESS) relieves obstruction of sinus drainage pathways with

Fig. 9.25 Meningeal invasion. In (**a**), this esthesioneuroblastoma has clearly breached the cribriform plate to enter the anterior cranial fossa. Although the thin dural enhancement (*arrowheads*) may be reactive in nature, the leptomeningeal enhancement (*arrows*) suggests meningeal invasion. In (**b**, **c**), in a patient with an undifferentiated carcinoma, vasogenic edema in the right frontal white matter (*asterisk*) indicates brain parenchymal invasion. (**d**) The graphic illustrates leptomeningeal invasion (*long arrow*), dural invasion (*short arrows*), and vasogenic edema from brain parenchymal invasion (*asterisk*)

reduced inflammation and improved mucociliary clearance (Fig. 9.31). Careful review of anatomic imaging before FESS is crucial to performing a safe and effective operation. Sinus CT clearly delineates the extent and location of disease but also defines the variable anatomy of the paranasal sinuses and key surrounding structures. While performing FESS is not reliant on real-time 3D image guidance, this technology can be assistive in more complex cases and/or when crucial anatomic landmarks are absent.

Preoperatively, the sinus CT should be used to delineate the anatomy of the skull base. As classified by Keros, the vertical height between the cribriform plate and fovea ethmoidalis is variable; as this measurement increases, so does the risk of

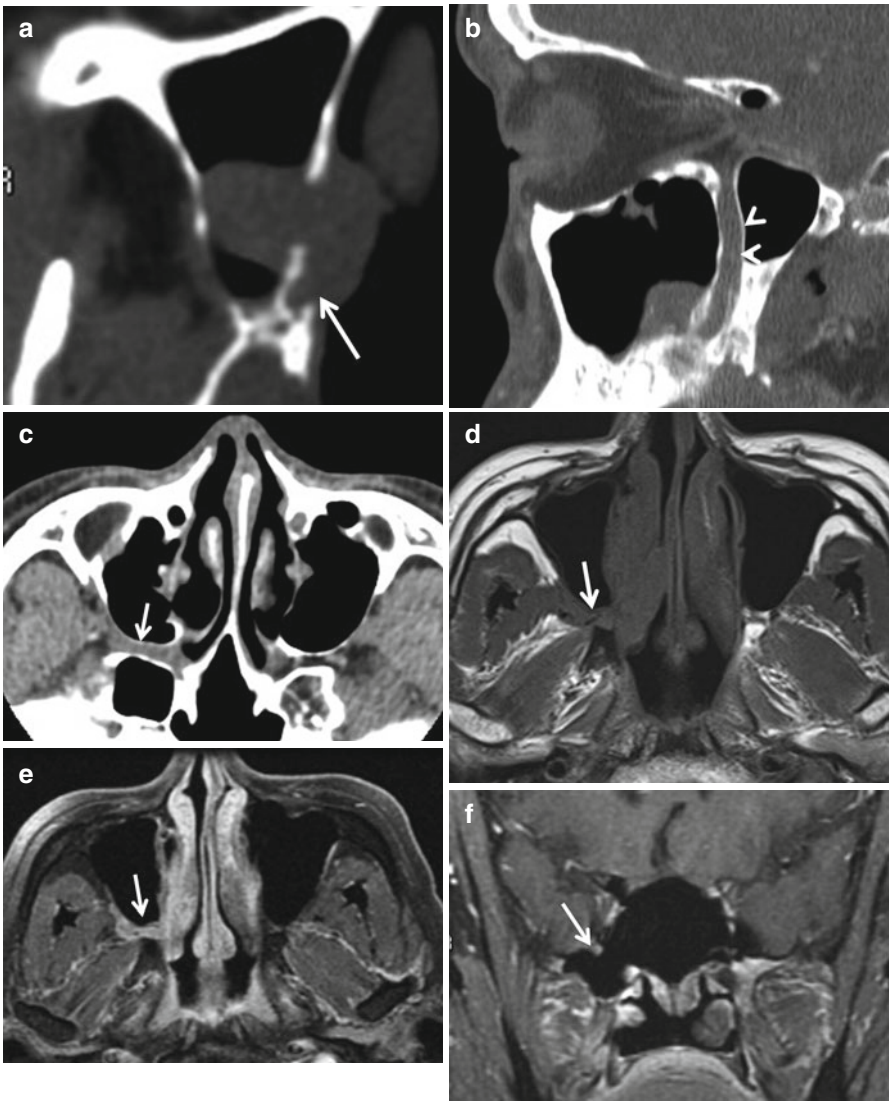

Fig. 9.26 Perineural spread of adenoid cystic carcinoma of the nasal cavity and maxillary sinus. In (**a**), the walls of the greater palatine nerve foramen are destroyed (*arrow*). In (**b**), spread of tumor along the length of the greater palatine nerve into the pterygopalatine fossa (PPF) is evident (*arrowheads*). In (**c**, **d**), note that although the fat density/signal intensity of the PPF is preserved on the left, it has been replaced with soft tissue on the right (*arrows*). Unenhanced T1-weighted images without fat suppression provide excellent depiction of soft tissue intensity tumor against a background of high signal fat. In (**e**), a fat-suppressed contrast-enhanced image, enhancement of tumor in the PPF is evident. In (**f**), note that there is enhancement and expansion of the right foramen rotundum indicating spread along the second division of the trigeminal nerve (*arrow*)

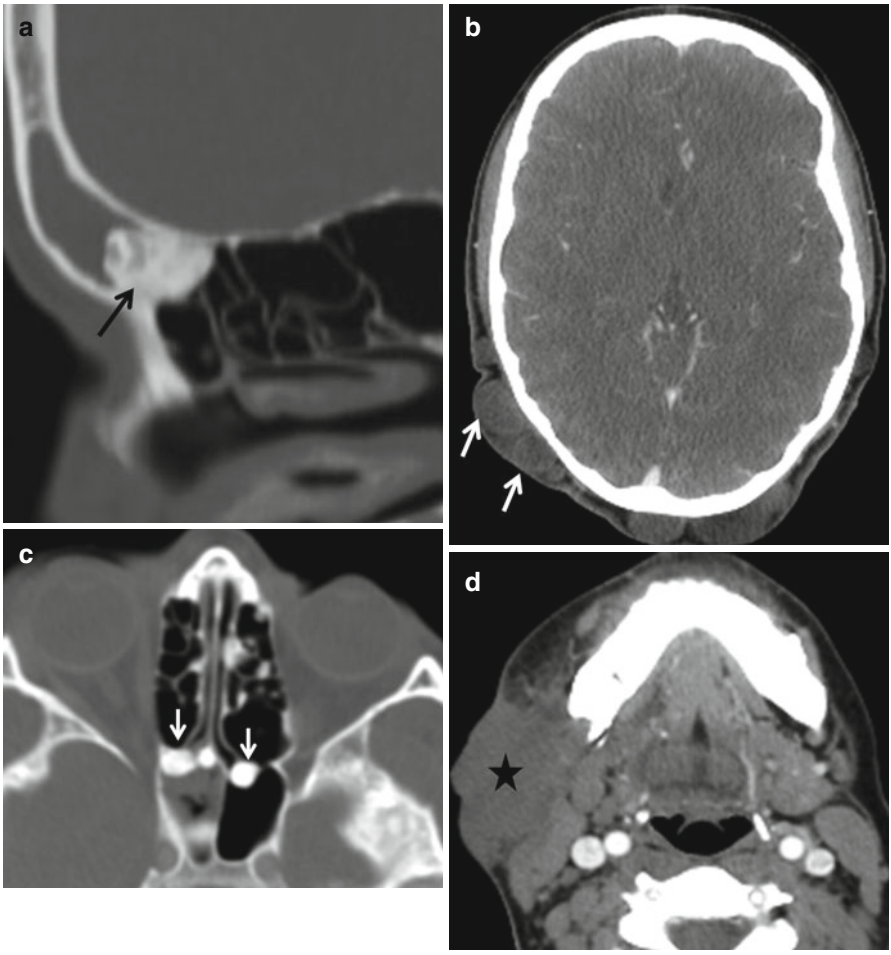

Fig. 9.27 (**a**) Osteoma causing obstruction of the frontal sinus drainage pathway. (**b–d**) Gardner's syndrome with multiple osteomas (*arrows*, **b**), sebaceous cysts (*arrows*, **c**), and a parotid space desmoid tumor (*asterisk*, **d**)

intraoperative skull base injury. Additionally, the superior skull base attachment of the middle turbinate should be noted, and the lamina papyracea should be evaluated for defects. The relationship of the ethmoid bulla to the lamina papyracea and the anterior skull base should be noted, as these landmarks are important for completion of a thorough ethmoidectomy. Identifying dehiscences of the internal carotid artery and optic nerve will help prevent inadvertent injury to these structures during the surgery. Positions of significant vessels that enter the nasal cavity including the anterior and posterior ethmoid arteries and the sphenopalatine artery should be noted.

Unusual air cells may harbor disease or create anatomic confusion when visualized transnasally, and an awareness of these variants is crucial. The CT scan can be used to identify conchae bullosa, Haller cells, agger nasi cells, supraorbital cells,

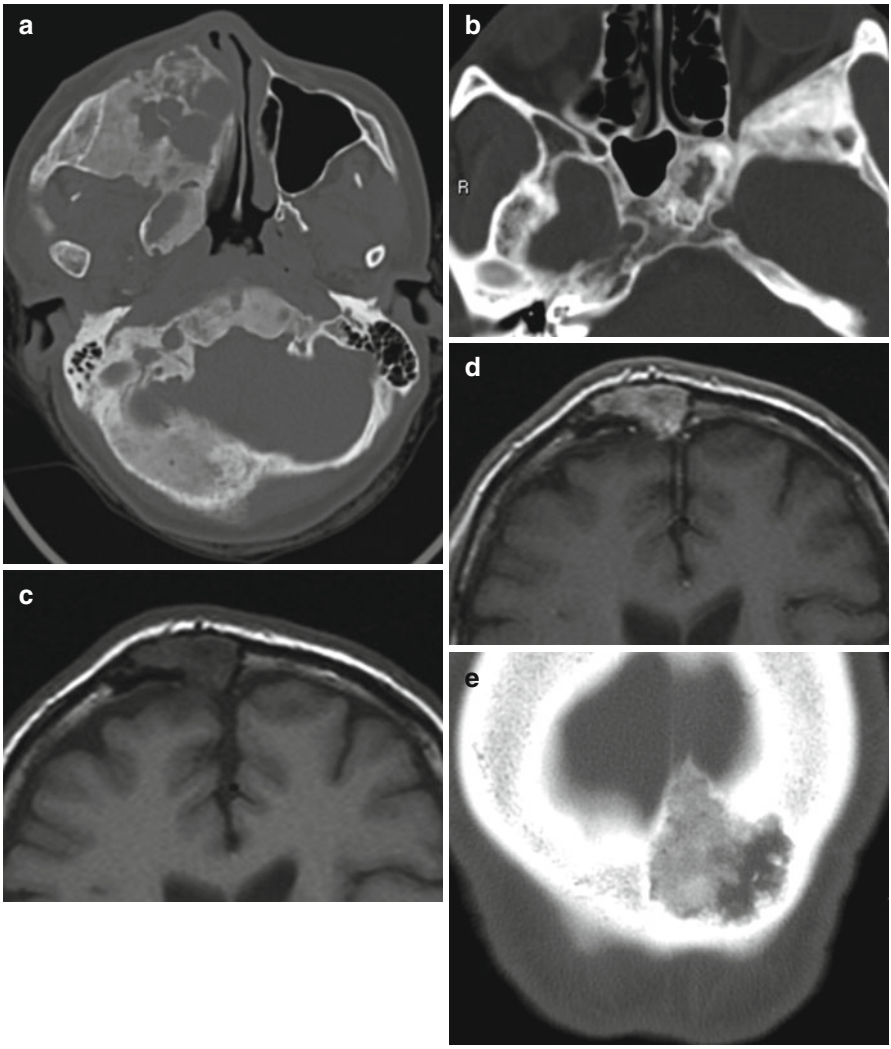

Fig. 9.28 Examples of fibrous dysplasia. In (**a**) the typical features of osseous expansion and involvement of multiple craniofacial bones is evident. In (**b**), the lesion in the left sphenoid sinus demonstrates a sclerotic rind while that in the left pterion is more homogeneously sclerotic. In (**c**, **d**), the lesion on MR simulates an aggressive lesion but the CT (**e**) reveals the ground glass matrix of typical fibrous dysplasia

and Onodi cells. For frontal sinus surgery, the position, orientation, and patency of the frontal outflow tract can be determined. Inter-sinus septa in the sphenoid and frontal sinuses, which are often not midline, should be examined. When correlated with physical exam findings, CT documentation of significant septal deviation and/or inferior turbinate hypertrophy can be useful in planning adjunctive procedures such as septoplasty and inferior turbinate fracture/reduction.

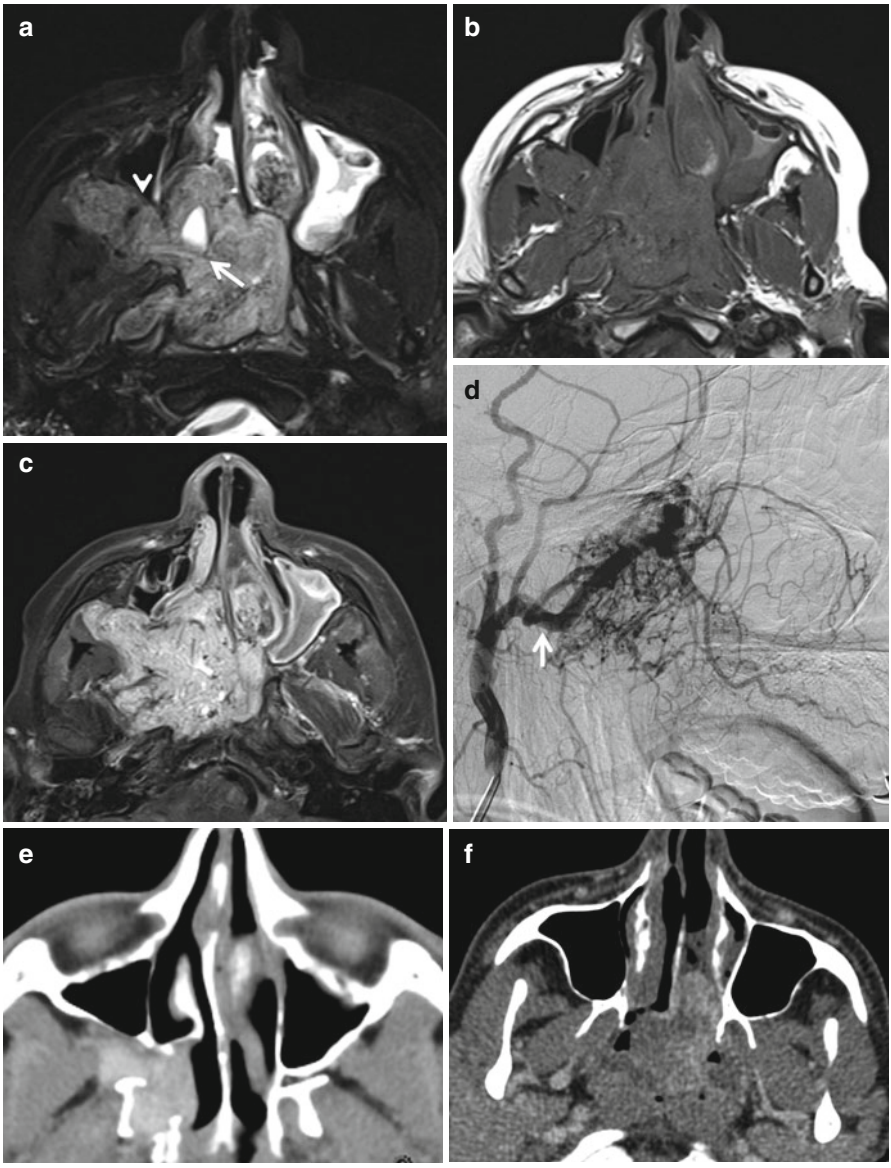

Fig. 9.29 Juvenile nasopharyngeal angiofibroma. Images (**a**–**d**) demonstrate the typical features of a JNA – a lesion centered at the sphenopalatine foramen (*arrow*), extension into the masticator space through the PPF with bowing of the posterior maxillary wall (*arrowhead*), and a large component in the nasal cavity accounting for epistaxis. Note the enlarged maxillary artery in (d) supplying the tumor. (**e**) Demonstrates the typical CT appearance of a JNA, that of an intensely enhancing lesion centered at the sphenopalatine foramen and extending into the PPF. (**f**) Is an atypical JNA in a 28-year-old patient. Note that the lesion lies entirely in the nasal cavity and enhances only moderately

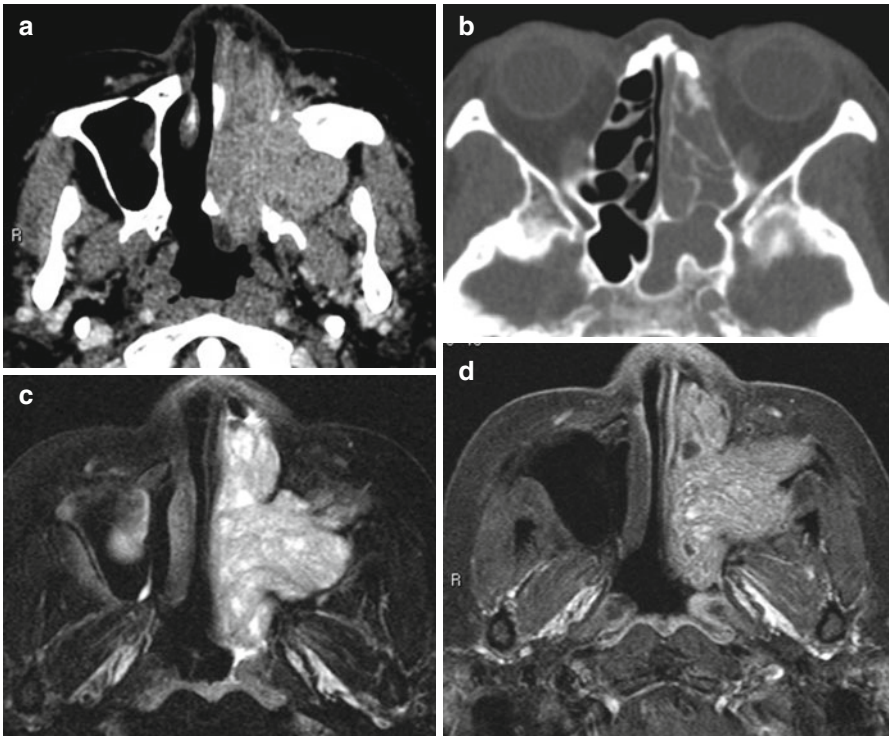

Fig. 9.30 Inverted papilloma in a middle-aged male smoker. An enhancing destructive mass is seen in the left nasal cavity and maxillary sinus. Although the CT appearance of this mass is nonspecific, the "cerebriform" pattern on the T2-weighted (**c**) and contrast-enhanced (**d**) MR image is highly suggestive of the diagnosis. Focal hyperostosis may indicate the site of origin of these tumors as seen in an anterior ethmoid cell in (**b**) (*arrow*)

Failure of FESS to resolve symptoms occurs in up to 20 % of patients (Fig. 9.31); possible causes are listed in Box 9.6. Box 9.7 summarizes the possible complications of FESS. CT is usually sufficient to evaluate these, but the optic nerves and meninges are best evaluated with MRI.

Box 9.6. Causes of Failed Functional Endoscopic Sinus Surgery

Postoperative obstructive synechia
Recurrent polyposis
Inadequate removal of agger nasi or frontal cells
Uncinate remnants
Lateralized middle turbinate
Osteitis of drainage pathway walls
Mucoceles

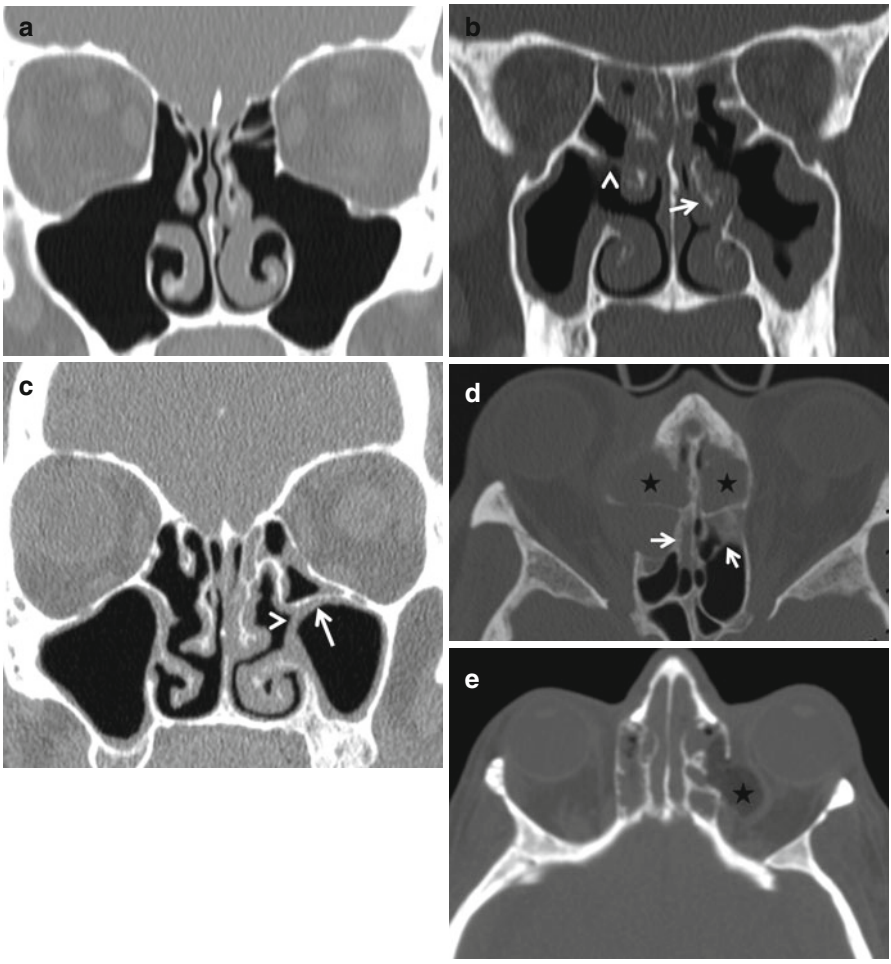

Fig. 9.31 Functional endoscopic sinus surgery. (**a**) Changes after bilateral uncinectomy and anterior ethmoidectomy. (**b**) Recurrent sinonasal polyposis after FESS. Note formation of synechia (*arrowhead*) and lateralization of the left middle turbinate (*arrow*). Persistent symptoms after FESS in (**c**). The left infundibulum is compromised by synechia (*arrowhead*) and an unaddressed Haller cell (*arrow*). The left middle turbinate is also adherent to the septum due to scarring (**d**). Persistent symptoms after FESS due to bilateral anterior ethmoid mucoceles (*asterisks*). Also seen are changes of chronic osteitis in the walls of the ethmoid air cells (*arrows*). In (**e**), inadvertent placement of packing material (*asterisk*) in the left orbit through a preexisting defect in the lamina papyracea is noted

Box 9.7. Complications of Functional Endoscopic Sinus Surgery

- Orbital
  - Intraorbital hematoma – anterior or posterior ethmoid artery injury
  - Extraocular muscle injury
  - Optic nerve injury
    - Direct trauma
    - Nerve compression by hematoma from PE artery injury
  - Nasolacrimal duct trauma
    - Dacryocystitis
    - Epiphora
- Vascular
  - Anterior and posterior ethmoid artery injury
  - Internal carotid artery injury
- Skull base
  - CSF leaks and recurrent meningitis
  - Meningoencephaloceles

9.5.2 Nasal Cavity and Sinus Tumors

While sinusitis is generally a bilateral disease, adults with unilateral nasal obstruction must be evaluated carefully for a tumor. In adults, a unilateral nasal mass that obscures the roof of the nasal vault should be imaged before a biopsy is performed to rule out a meningoencephalocele. This is best done with MRI. When appropriate, biopsy is important to determining treatment approach because imaging characteristics are often inadequate to predict a definitive diagnosis. While benign expansile lesions can be destructive, CT and MRI can generally delineate benign from malignant tumors, and most benign tumors today will be managed using endoscopic surgery. However, management of malignant nasal cavity and sinus tumors is highly variable depending on the location and the histology. In general, management is most impacted by the extent of local disease. Major factors include extension beyond the nasal and sinus cavities, particularly into the cranial vault, orbit, or nasopharynx. Again, it is important to determine invasion into and through these structures versus erosion by a benign expansile mass. Once intracranial, it is important to determine the presence and degree of dural and parenchymal involvement. With more extensive malignant lesions, neck imaging may be appropriate to evaluate for regional metastases.

Resection of malignant tumors involving the superior nasal vault can be performed by open (i.e., craniofacial), endoscopic, or combined approaches. Immediate postoperative CT imaging often shows thick enhancement of the frontal dura, a reactive phenomenon that must not be mistaken for infection or tumor. Pericranial or myofascial flaps are commonly used to fill the skull base defect; these can demonstrate a convex masslike appearance on imaging for an extended

period of time. The presence of a walled-off fluid collection on a postoperative scan is not normal and may indicate infection, hematoma, or a CSF leak (Fig. 9.32). Likewise, postoperative enhancement is usually linear and smooth; any nodularity, especially if it increases in size on serial imaging, must be presumed to represent recurrent tumor.

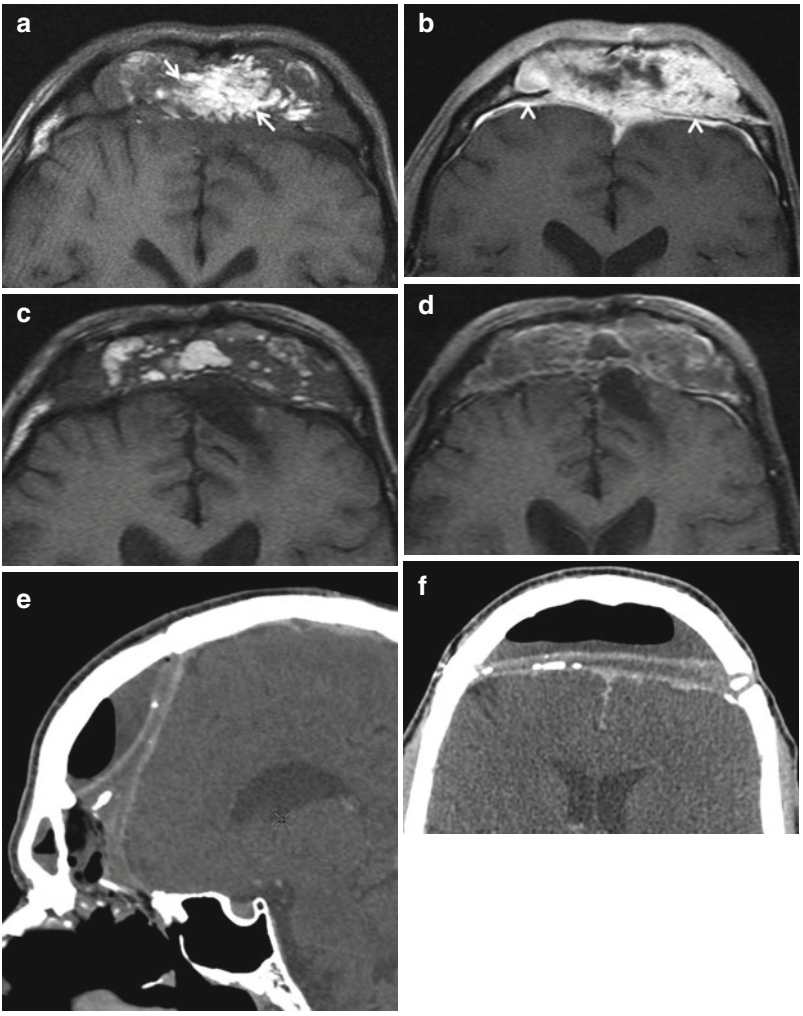

Fig. 9.32 Postoperative findings after craniofacial resection for esthesioneuroblastoma. Images (**a**, **b**) were obtained immediately after surgery, while (**c**, **d**) are from a study 6 months after the procedure. Note the persistent masslike appearance of the myofascial flap. The T1 hyperintense foci (*arrows*), representing fat involute with time. Enhancement of the flap and of the underlying dura (*arrowheads* in **b**) is not unusual and subsides with time. The presence of a fluid collection or of air-fluid levels (**e**, **f**) is not an expected postoperative finding and may indicate infection as in this case

Further Reading

Aribandi M, McCoy VA, Bazan C (2007) Imaging features of invasive and noninvasive fungal sinusitis: a review. Radiographics 27(5):1283–1296

Daniels DL, Mafee MF, Smith MM, Smith TL, Naidich TP, Brown WD, … Strottmann JM (2003) The frontal sinus drainage pathway and related structures. Am J Neuroradiol 24(8): 1618–1627

Eden BV, Debo RF, Larner JM, Kelly MD, Levine PA, Stewart FM, Cantrell RW, Constable WC (2006) Esthesioneuroblastoma. Long term outcome and patterns of failure—the University of Virginia experience. Cancer 73(10):2556–2562

Hoang JK, Eastwood JD, Tebbit CL, Glastonbury CM (2010) Multiplanar sinus CT: a systematic approach to imaging before functional endoscopic sinus surgery. Am J Roentgenol 194(6):W527–W536

Huang BY, Lloyd KM, DelGaudio JM, Jablonowski E, Hudgins PA (2009) Failed endoscopic sinus surgery: spectrum of CT findings in the frontal recess. Radiographics 29(1):177–195

Raghavan P, Phillips CD (2007) Magnetic resonance imaging of sinonasal malignancies. Top Magn Reson Imaging 18(4):259–267

Schuster JJ, Phillips CD, Levine PA (1994) MR of esthesioneuroblastoma (olfactory neuroblastoma) and appearance after craniofacial resection. AJNR Am J Neuroradiol 15(6):1169–1177

Yousem DM, Gad K, Tufano RP (2006) Resectability issues with head and neck cancer. AJNR Am J Neuroradiol 27(10):2024–2036